Chapter 5

ULTIMATE BEARING CAPACITY FACTORS FOR RING FOOTING ON TWO LAYERED SOILS DUE TO VARIOUS LOADING POSITIONS

5.1 INTRODUCTION

Chapter 4 addresses the behaviour of ring footings resting on two layered soils. Due to its high load-withstanding ability and lesser usage of construction material, the ring footing appears to be a technically effective and economically beneficial substructure for supporting axisymmetric super-structures. The literature review presented in the preceding chapter suggests that the ultimate bearing capacity (UBC) of ring foundations on homogenous as well as multi-layered soil systems was examined through different techniques. But, truly speaking, the existing literature pertaining to ring foundations is considerably limited in contrast to the extensive amount of research available on the strip, rectangular, and circular footing. Furthermore, almost all studies on the ring foundation were conducted by considering the vertical load to be uniformly distributed over the entire footing surface. Nevertheless, there are a few occasions where the vertical symmetric loading is applied partially over the annular section. And, the position of the partial load can also be different. Hence, the computation of the UBC of the ring footing by varying the position of the partial load is a practical problem in the field of geotechnical engineering. Vali et al. (2019) pioneered in examining the effect of partial loading on the bearing capacity of ring footing. By using FELA software Optum G2, they rigorously examined the effect of four differently-placed partial loading on the behaviour of smooth and rough ring footing located on homogenous frictional and cohesive soils. The study reported that the outer half loading

and the inner half loading are the optimal loading position for ring foundations when placed over cohesive and frictional soil, respectively.

However, no rigorous and extensive work is found to exist for determining the bearing capacity of ring footing placed over two-layered soils by duly considering the effect of different loading positions. In this study, an attempt has been made to determine the effect of various loading positions on the bearing capacity of ring footings resting over three different layered soils: (a) sand over sand, (b) clay over clay, and (c) sand over clay. The analyses are carried out by employing the axisymmetric lower-bound limit analysis with finite elements and nonlinear optimization. In some construction sites, ring footings subjected to partial vertical loadings need to be constructed on weak clay deposits whose load-bearing capacity can be improved by laying a relatively stronger coarse-grained layer between the footing and the clay surface. And, therefore, the present study is further extended to investigate the strength improvement of the partially loaded ring footings with respect to the bearing capacity failure due to the inclusion of the sand layer beneath the ring foundation. The combined impacts of various factors such as radius ratio, upper-layer thickness, surcharge pressure, upper- and lower-layer soil strength, loading positions, and footing roughness are extensively scrutinized.

5.2 PROBLEM STATEMENT AND DOMAIN

A rigid ring footing, having an external radius, r_0, and an internal radius, r_i, is resting over two layered soils. The soil profile is considered to consist of either of the three combinations: (a) two layers of sand, (b) two layers of clay, and (c) a sand layer resting over clayey stratum. The sand layers are considered to be drained and the clayey layers are assumed to be completely saturated and undrained. The top and the bottom layer are having different shear strength parameters. The strength properties of each

layer are further assumed to be homogenous, isotropic, and stress-independent. The ground surface on which the footing is placed is kept to be horizontal. It is intended to compute the ultimate bearing capacity (UBC) of smooth as well as rough ring footing by placing the load at three different specific positions, namely, i) inner half (L_1), ii) middle half (L_2), and iii) outer half (L_3). The comparisons are drawn with complete loading condition (L_0). The loading positions are depicted in Figure 5.1c. A wide range of ring geometry, soil profiles, and surcharge pressure are considered in the analysis.

Owing to the symmetricity of the problem, a planar domain in *r-z* plane is employed by keeping the axis of the symmetry as one of its vertical boundaries. The problem domain is chosen sufficiently large enough so that (a) the solution does not get affected by any further extension of the domain size and (b) the failure zone is contained well within the defined domain boundaries. The presence of surcharge loading and laying of strong soil layers enhances the domain size requirement to an appreciable extent. The surcharge pressure acts normal to ground surface. The stress boundary conditions that are imposed in the problem are as follows:

(i) along the axis of symmetry (AB): $\tau_{rz} = 0$,

(ii) along the ground surfaces (AM and ND): $\tau_{rz} = 0$ and $\sigma_z = -q$, and

(iii) along the soil–footing interface (MN): $|\tau_{rz}| \leq (c\cot\phi - \sigma_z)\tan\delta$; where δ = interface friction angle between the footing base and the soil mass. This condition arises due to the fact that the shear stress along the soil–footing interface will act to oppose the movement of the soil particles and that there would not be any point along the soil–footing interface where the magnitude of the mobilized shear stress exceeds the shear strength of the soil. The modulus sign is employed over the shear stress component, and although this is not necessary, it reduces the computational time. In the case of a

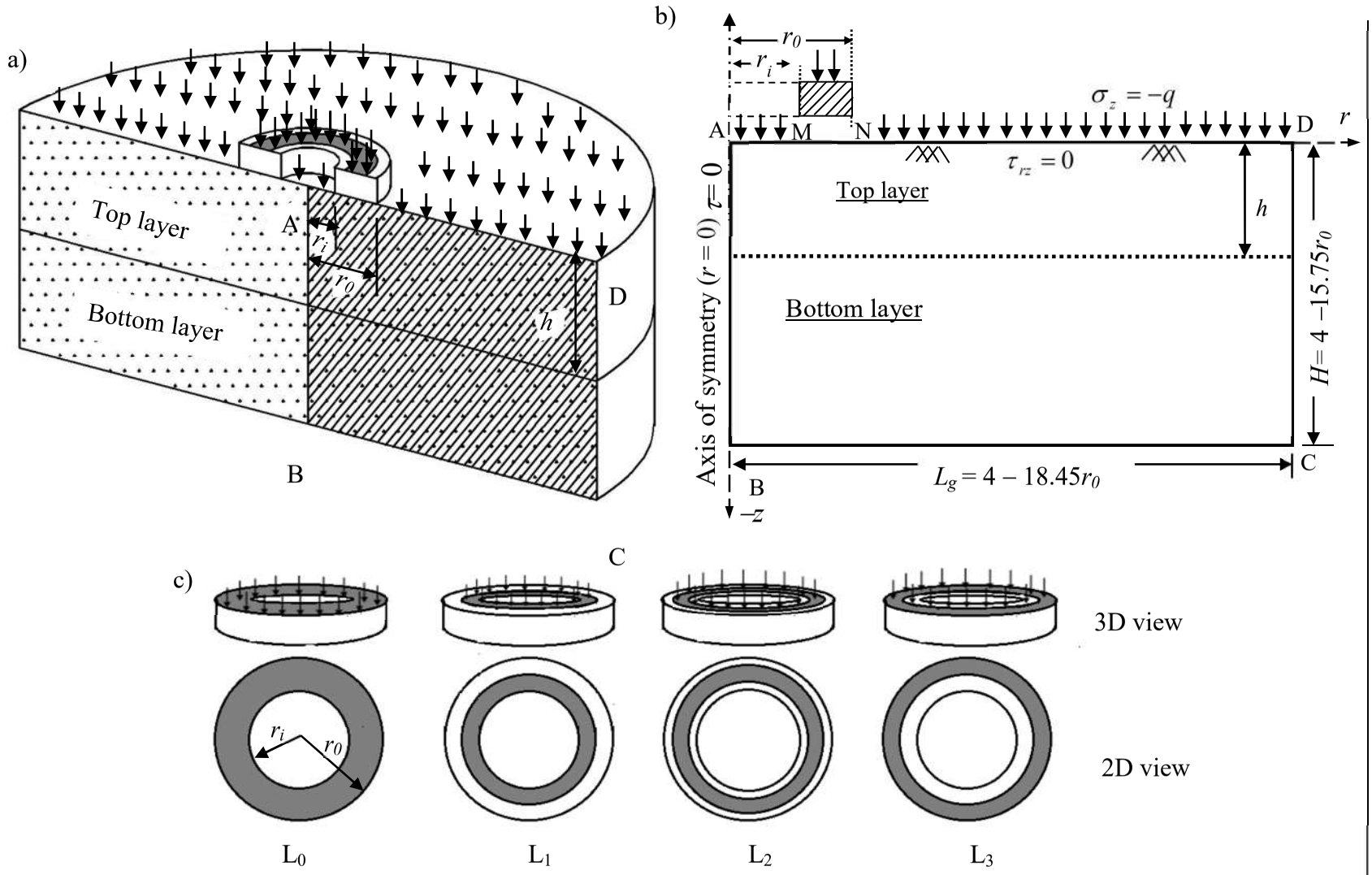

Figure 5.1 Ring footing rested over two layered, as represented in a) three-dimensional axisymmetric form, b) two-dimensional form; and c) three different configurations of loadings.

perfectly smooth footing, no shear stress acts along the interface ($\delta = 0°$), whereas in the case of a perfectly rough footing, the mobilized shear stress should not be more than shear strength ($\delta = \phi$).

Figure 5.1b illustrates the chosen domain and the associated stress boundary conditions. The domain is first discretized with three nodded linear strain triangular element and each node of an element is assigned with four unknown stress variables (σ_r, σ_z, σ_θ, and τ_{rz}). Figure 5.2 shows the chosen mesh for four different radius ratios. The concentration of elements near the footing edge is kept to be very high for capturing the singularity.

5.3 RESULTS AND DISCUSSION

In the present study, the simulations are carried out for the following cases:

A) Geometrical Properties: (i) Radius ratio (r_i/r_0) = 0, 0.25, 0.50, 0.75, and 0.90.
(ii) Depth ratio (h/r_0) = 0.125, 0.25, 0.5, 1, 2, and 5.

B) Material Strength Properties:

Sand over Sand (S-S case): ϕ_1= 30°, 35°, 40°, 45° ϕ_2 = 30°, 35°, 40°, 45°

Clay over Clay (C-C case): $c_{u1}/(\gamma r_0)$ = 0.25, 0.5, 1,2 $c_{u2}/(\gamma r_0)$ = 0.25, 0.5, 1, 2

Sand over Clay (S-C case): ϕ =30°, 35°, 40°, 45° $c_u/(\gamma r_0)$ = 0.25, 0.5, 1, 2

C) Soil-Footing Interface Angle (δ) : 0° and ϕ

D) Surcharge pressure: $(q/(\gamma r_0))$ = 0 and 1.

E) Loading Positions on the Ring Footing: Complete loading (L_0),
Inner-half loading (L_1),
Middle-half loading (L_2), and
Outer-half loading (L_3).

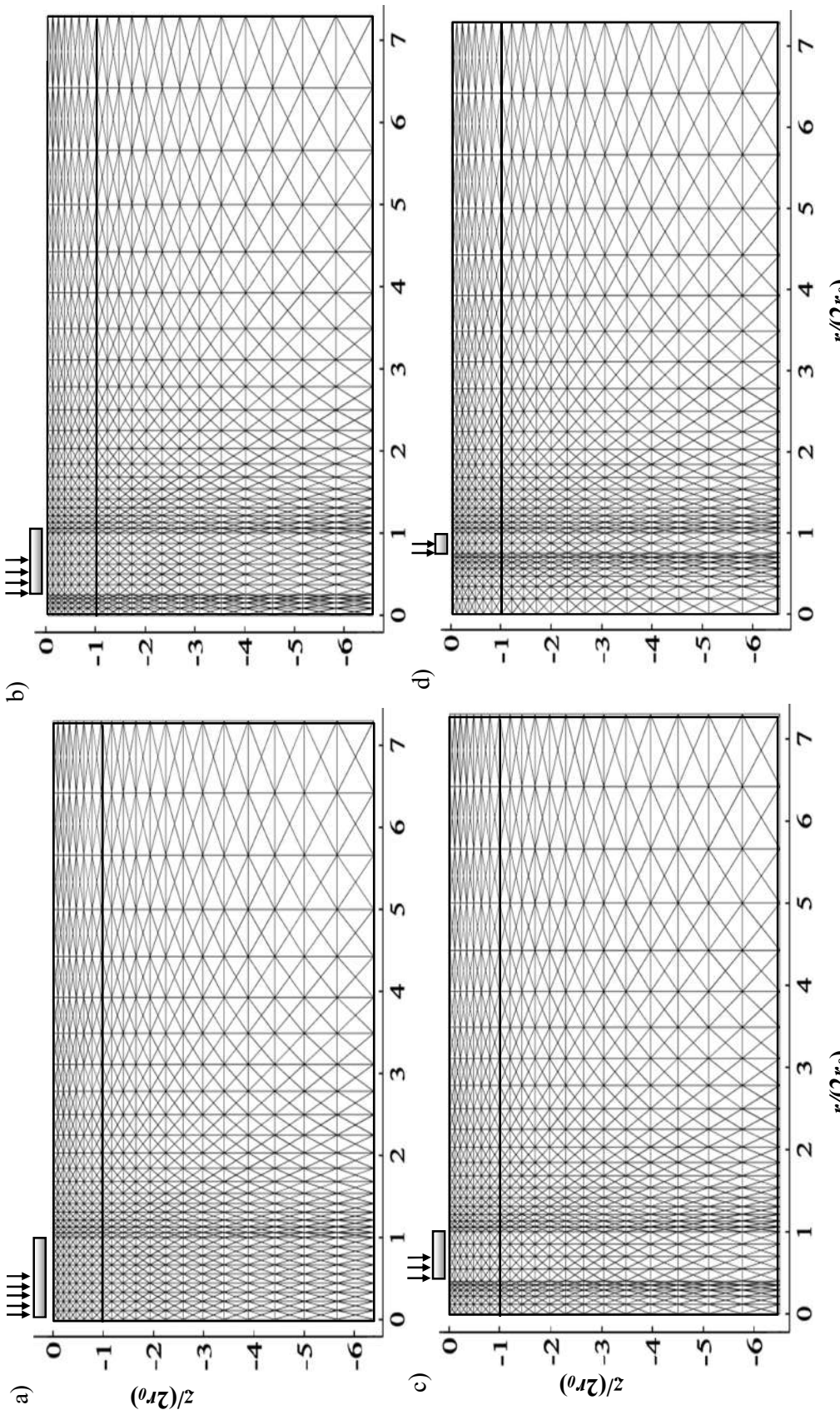

Figure 5.2 Mesh used for the ring footing corresponding to ϕ_1=30°, ϕ_2=35°, and for four different radius ratios: a) r_i/r_0= 0; b) r_i/r_0= 0.25; c) r_i/r_0= 0.50; and d) r_i/r_0= 0.75.

5.3.1 For homogenous soil:

Table 5.1 presents the magnitude of the UBC (p_u) of the ring footing resting on homogenous soils. The magnitude of p_u increases with the increase in soil strength and surcharge loading. The numerical solutions give an impression that for the specific strength parameters and surcharge loadings, p_u is minimum for L_0 conditions and maximum for L_1 conditions. For undrained clays, barring L_3 conditions, p_u decreases with the increase in the radius ratio (r_i/r_0) irrespective of the surcharge pressure. Conversely, for L_3 loadings, p_u continuously increases as the width of the annular section reduces. For higher friction angle with surcharge loading, the magnitude of p_u initially increases with r_i/r_0 ratio and then subsequently decreases; thus, it provides a certain r_i/r_0 ratio (referred to here as *critical radius ratio*, $r_i/r_0\big|_{cr}$), at which the bearing capacity is found to be maximum. The existence of $r_i/r_0\big|_{cr}$ is not visible for the L_1 condition. The impact of the surcharge on the magnitude of p_u is more for frictional soil as compared with cohesive soil. For frictional soil, the trend of the variation of p_u with respect to radius ratio depends not only on the loading condition but also on the surcharge pressure. For example, corresponding to L_3 configuration, the application of surcharge pressure results in the existence of $r_i/r_0\big|_{cr}$ for $\phi \geq 30°$ soil, whereas in the absence of surcharge pressure, $r_i/r_0\big|_{cr}$ is not present even when $\phi = 40°$.

It is to be further noted that although the load intensity for various loading position varies significantly, as long as the load is symmetrically placed, the magnitude of the vertical collapse load evaluated at the center of the footing will remain the same regardless of loading configuration; this observation can also be interpreted from the work of Vali et al. (2019). The present chapter depicts the variation of load intensity for various layered soils and provides a general guideline of how the load is to be placed over the ring footing for maximum benefits from the viewpoint of load-withstanding

Table 5.1. The ultimate bearing capacity (p_u) of ring footing placed on homogenous sands and clays for different combination of r_i/r_0, $q/(\gamma r_0)$ and loading positions.

Loading Positions	r_i/r_0	$c_u/(\gamma r_0)$								ϕ							
		0.25		0.5		1		2		30°		35°		40°		45°	
		$q/(\gamma r_0)$								$q/(\gamma r_0)$							
		0	1	0	1	0	1	0	1	0	1	0	1	0	1	0	1
L_0	0	1.5	2.5	3.0	4.0	6.0	7.0	12.0	13.0	15.1	58.9	40.2	135.2	116.0	345.1	379.1	998.4
	0.25	1.5	2.5	2.9	3.9	5.9	6.9	11.7	12.7	9.7	56.8	28.2	139.9	93.3	367.8	368.6	1062.4
	0.5	1.4	2.4	2.8	3.8	5.5	6.5	11.1	12.1	4.9	39.2	12.9	89.9	38.8	237.2	140.8	753.6
	0.75	1.3	2.3	2.6	3.6	5.3	5.3	10.6	11.6	2.1	26.9	5.1	55.0	13.4	126.1	40.3	336.2
L_1	0	6.0	10.2	12.0	16.0	24.1	28.1	48.2	52.2	60.6	235.4	160.5	541.5	463.6	1380.3	1516.4	3977.3
	0.25	4.2	7.0	8.4	11.2	16.8	19.6	33.5	36.4	27.6	162.1	80.7	397.5	267.6	1050.4	1043.5	3030.9
	0.5	3.3	5.7	6.7	9.1	13.3	15.7	26.6	29.0	11.8	93.8	31.1	215.8	93.4	569.0	337.6	1809.0
	0.75	2.9	5.0	5.7	7.9	11.4	13.6	22.9	25.0	4.5	57.8	10.9	118.7	28.6	271.9	88.1	724.9
L_2	0	3.0	5.0	6.0	8.0	12.0	14.1	24.1	26.1	30.4	117.7	80.4	270.5	231.8	688.5	756.3	1985.8
	0.25	2.9	4.9	5.9	7.9	11.7	13.7	23.4	25.4	19.6	113.4	57.0	280.2	189.9	736.4	738.4	2139.1
	0.5	2.8	4.8	5.6	7.5	11.1	13.1	22.2	24.2	10.0	78.4	26.1	179.9	78.8	476.7	288.1	1498.2
	0.75	2.7	4.7	5.3	7.3	10.6	12.4	21.2	23.2	4.2	53.7	10.3	110.3	26.5	253.6	82.5	680.8
L_3	0	2.0	3.3	4.0	5.3	8.0	9.4	16.1	17.4	20.0	78.2	52.9	180.6	152.5	457.4	502.8	1337.5
	0.25	2.3	3.8	4.5	6.0	9.0	10.6	18.0	19.6	14.8	87.2	43.5	215.3	143.6	567.4	570.6	1642.6
	0.5	2.4	4.1	4.8	6.5	9.5	11.2	19.0	20.7	8.4	67.1	22.2	154.1	66.6	406.1	243.2	1287.5
	0.75	2.5	4.3	5.0	6.8	9.9	11.8	19.8	21.7	3.9	50.2	9.5	102.7	24.9	235.8	75.7	631.6

capacity.

5.3.2 For two-layered soil:

5.3.2.1 Case 1: Sandy layer underlain by another sandy layer (S-S case)

The analyses were performed for two different combinations of sand layers – weak over strong (Type A1) as well as strong over weak (Type A2). Figures 5.3–5.10 depict the variation of normalized bearing capacity ($p_u/\gamma(r_0-r_i)$) with respect to the radius ratio (r_i/r_0). It is well observed that in the absence of surcharge pressure, after a specific radius ratio (designated here as $r_i/r_{0|sp}$) the curves start to converge for both smooth as well as rough footing. It indicates that beyond $r_i/r_{0|sp}$, the bearing capacity is solely governed by the strength of the top layer. The existence of $r_i/r_{0|sp}$ becomes more prominent for Type A1 soil and its magnitude significantly decreases with the increase in h/r_0.

It is further noted that for any specific combinations of soil properties and ring geometry, corresponding to zero surcharging, UBC always becomes maximum for L_1 and minimum for L_3; however, regardless of the loading positions, the curves show a decreasing trend. The decreasing trend is preceded by the horizontal plateau, especially for the L_3 loading and rough footing. However, in the presence of surcharge pressure, the nature of the normalized bearing capacity curves is highly influenced by the loading positions. With the narrowing of the annular section, the normalized value of p_u, considering surcharge pressure, either increases for Type A2 soil, especially for the rough ring footing, corresponding to L_2 and L_3 loading conditions, or significantly decreases for Type A1 soil corresponding to L_1 conditions. It can be inferred from these observations that the annular footing is far more beneficial than the circular one if the loading position is of L_2 or L_3 type and the surcharge pressure is applied over soil Type A2. The normalized p_u becomes higher for L_1 followed by L_2 and then followed by L_3

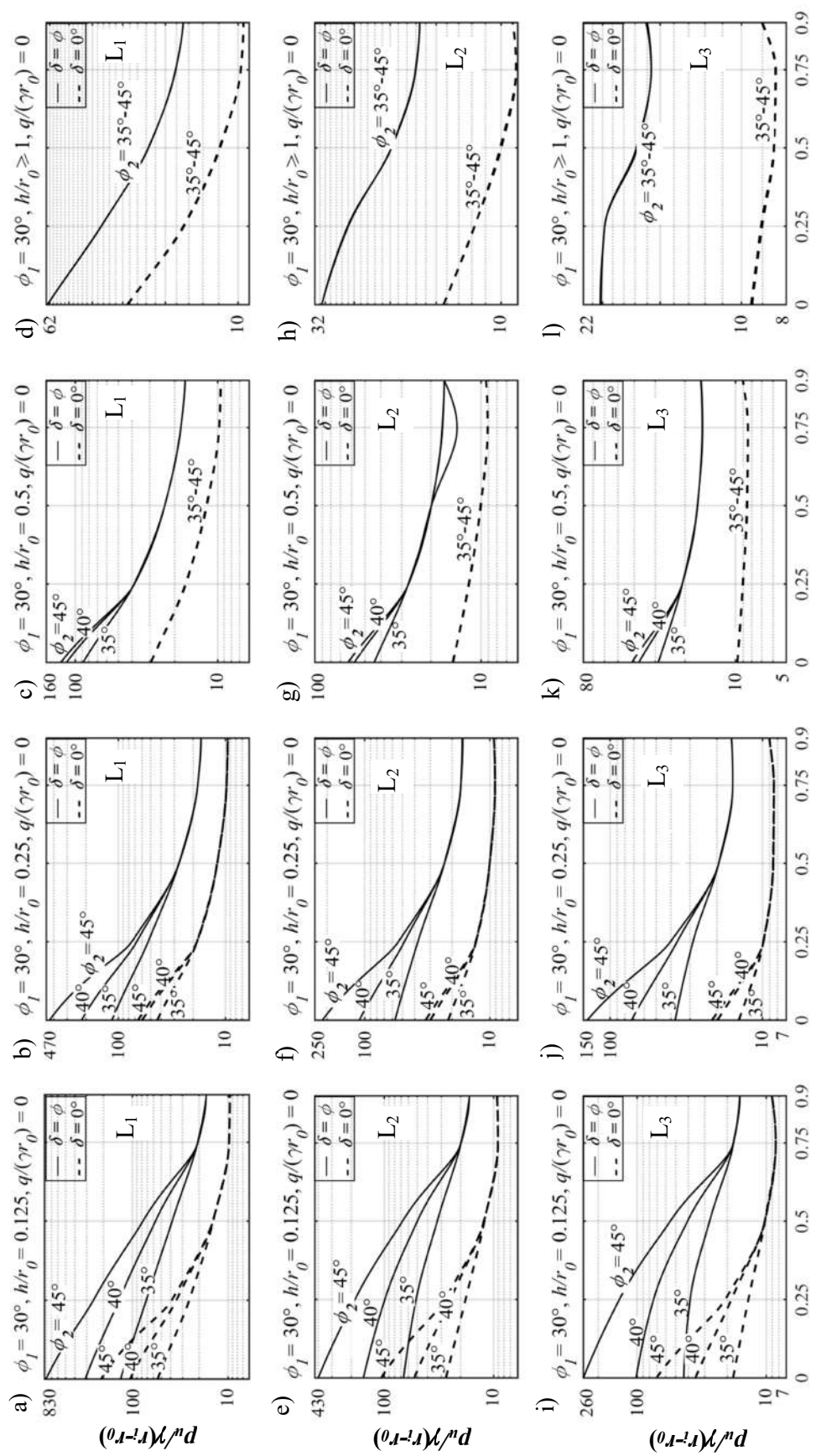

Figure 5.3 The variations of normalized bearing capacity with respect to r_i/r_0 for smooth and rough ring footing resting on a sand layer having ϕ_1=30° and different values of ϕ_2 with $q/(\gamma r_0)$=0 and corresponding to three different loading positions: (a–d) L_1; (e–h) L_2; and (i–l) L_3.

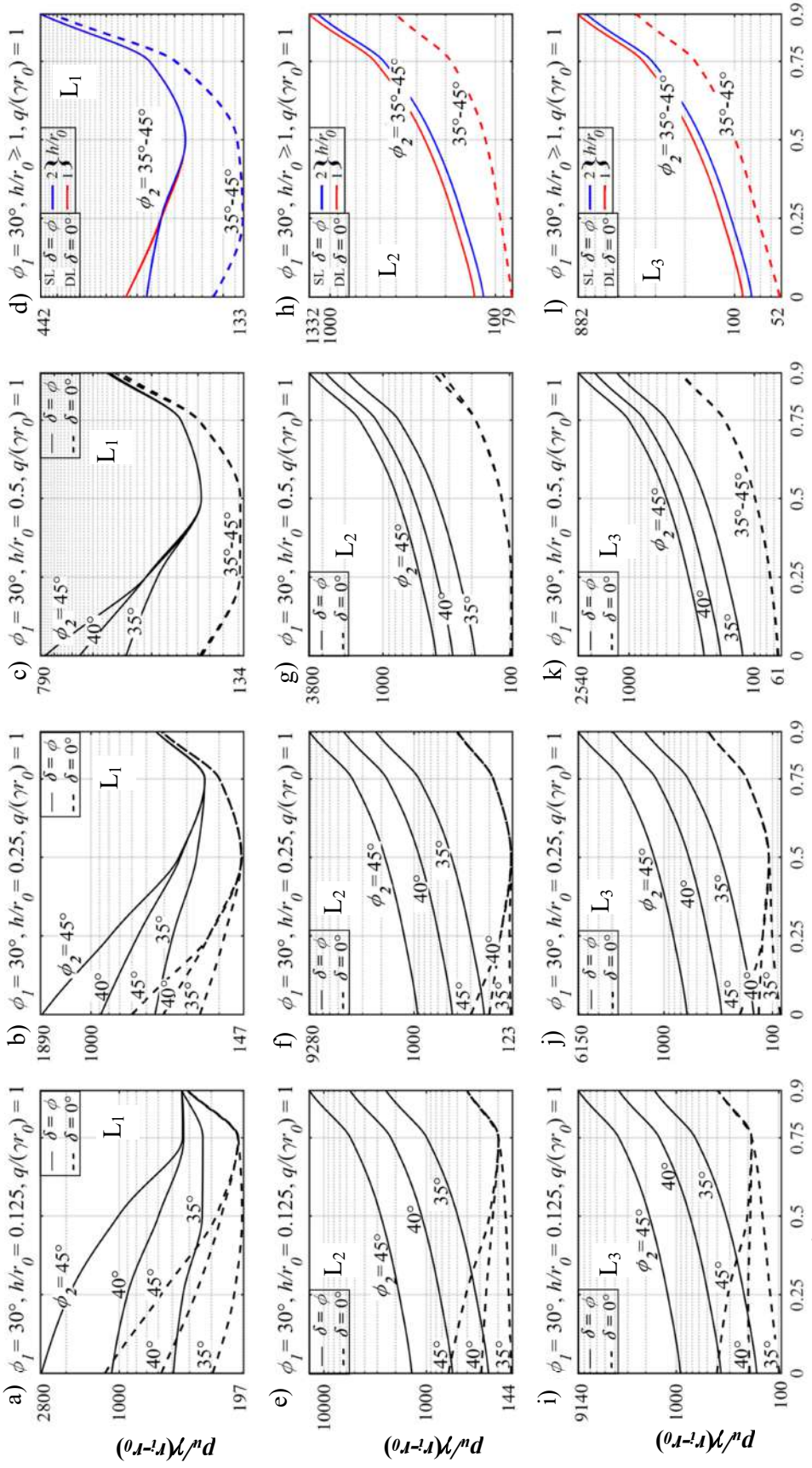

Figure 5.4 The variations of normalized bearing capacity with respect to r_i/r_0 for smooth and rough ring footing resting on a sand layer having ϕ_1=30° and different values of ϕ_2 with $q/(\gamma r_0)$=1 and corresponding to three different loading positions: (a–d) L_1; (e–h) L_2; and (i–l) L_3. SL: solid line; and DL: dashed line.

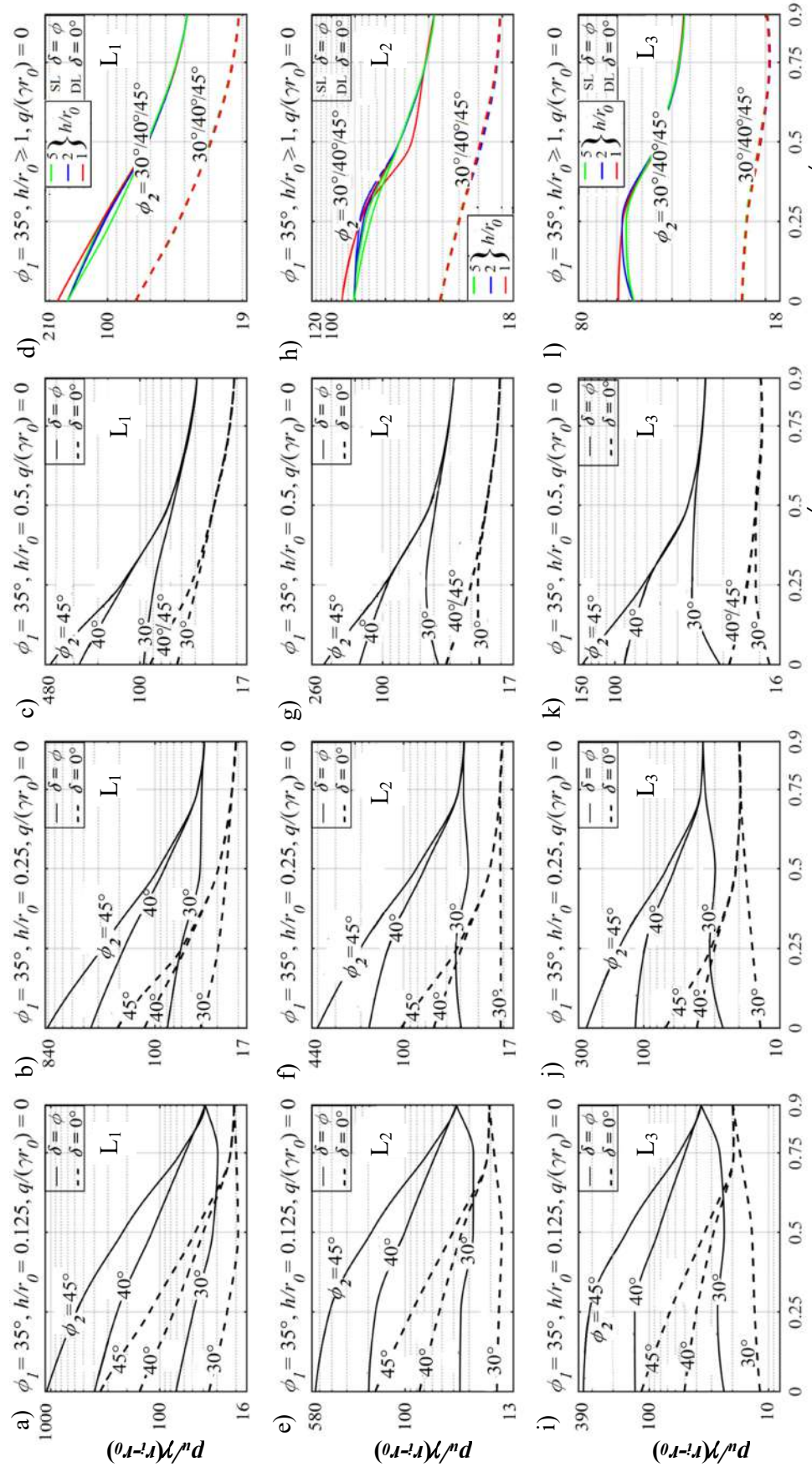

Figure 5.5 The variations of normalized bearing capacity with respect to r_i/r_0 for smooth and rough ring footing resting on a sand layer having ϕ_1=35° and different values of ϕ_2 with $q/(\gamma r_0)$=0 and corresponding to three different loading positions: (a–d) L_1; (e–h) L_2; and (i–l) L_3. SL: solid line; and DL: dashed line.

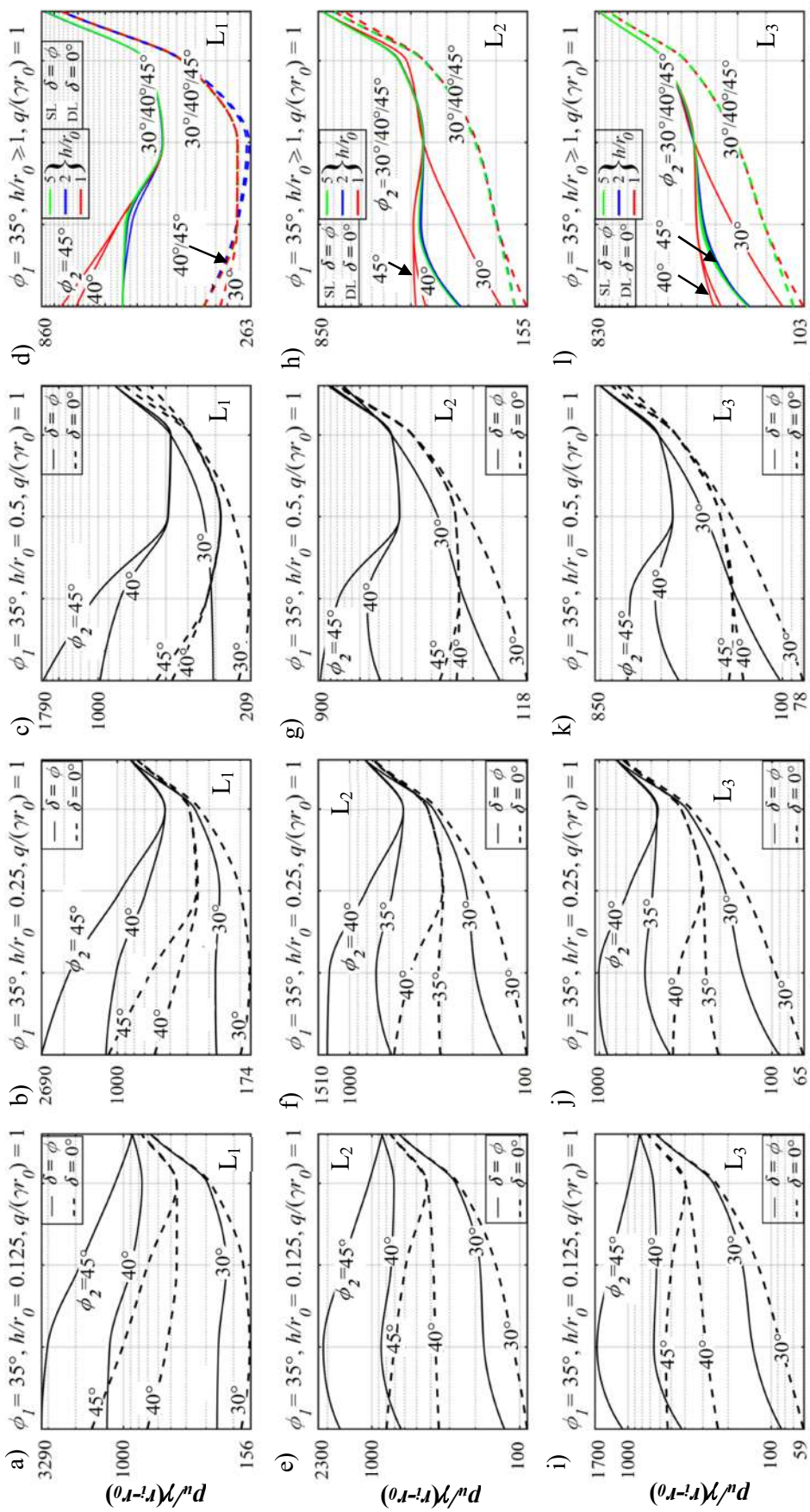

Figure 5.6 The variations of normalized bearing capacity with respect to r_i/r_0 for smooth and rough ring footing resting on a sand layer having ϕ_1=35° and different values of ϕ_2 with $q/(\gamma r_0)$=1 and corresponding to three different loading positions: (a–d) L_1; (e–h) L_2; and (i–l) L_3. SL: solid line; and DL: dashed line.

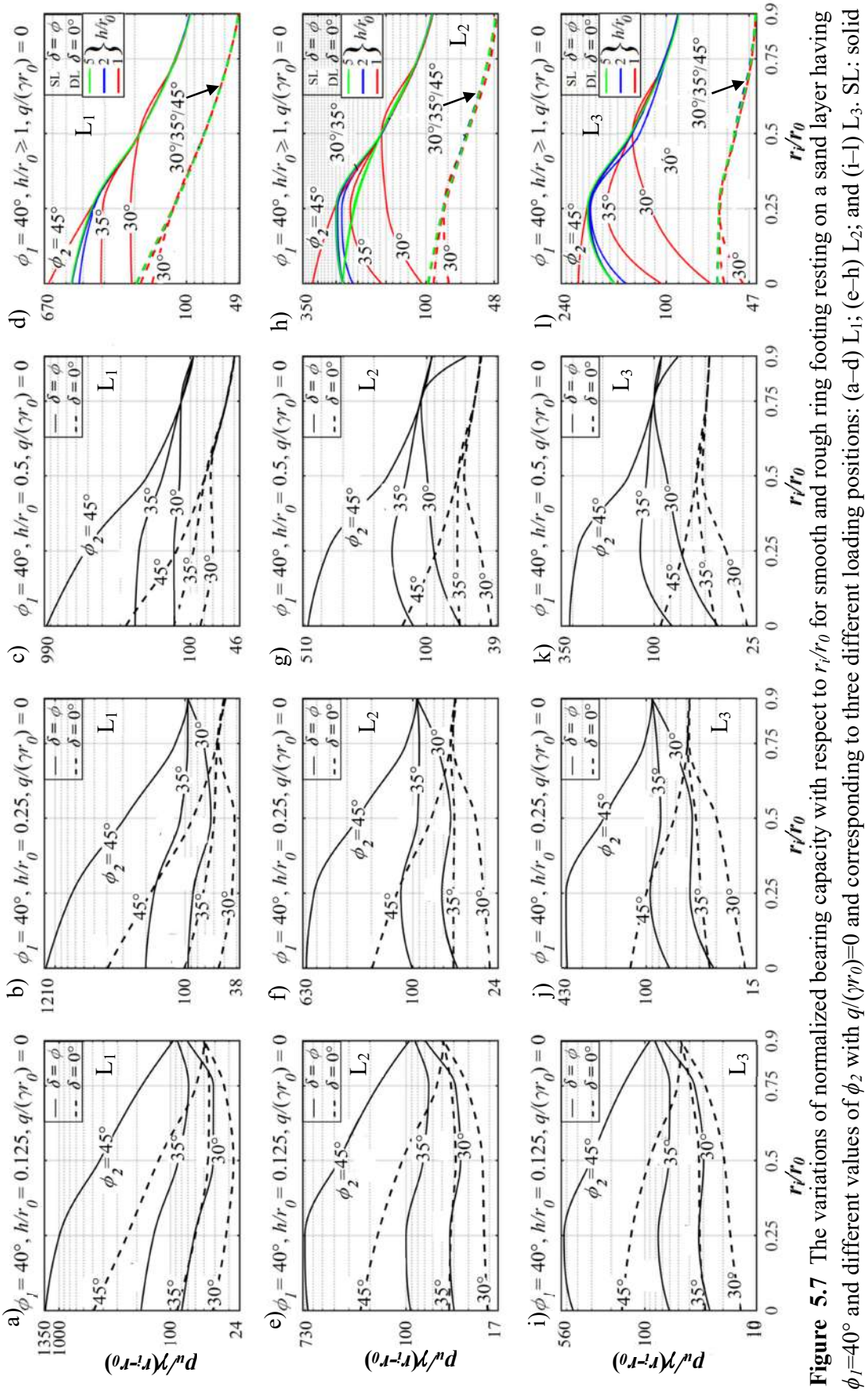

Figure 5.7 The variations of normalized bearing capacity with respect to r_i/r_0 for smooth and rough ring footing resting on a sand layer having ϕ_1=40° and different values of ϕ_2 with $q/(\gamma r_0)$=0 and corresponding to three different loading positions: (a–d) L_1; (e–h) L_2; and (i–l) L_3. SL: solid line; and DL: dashed line.

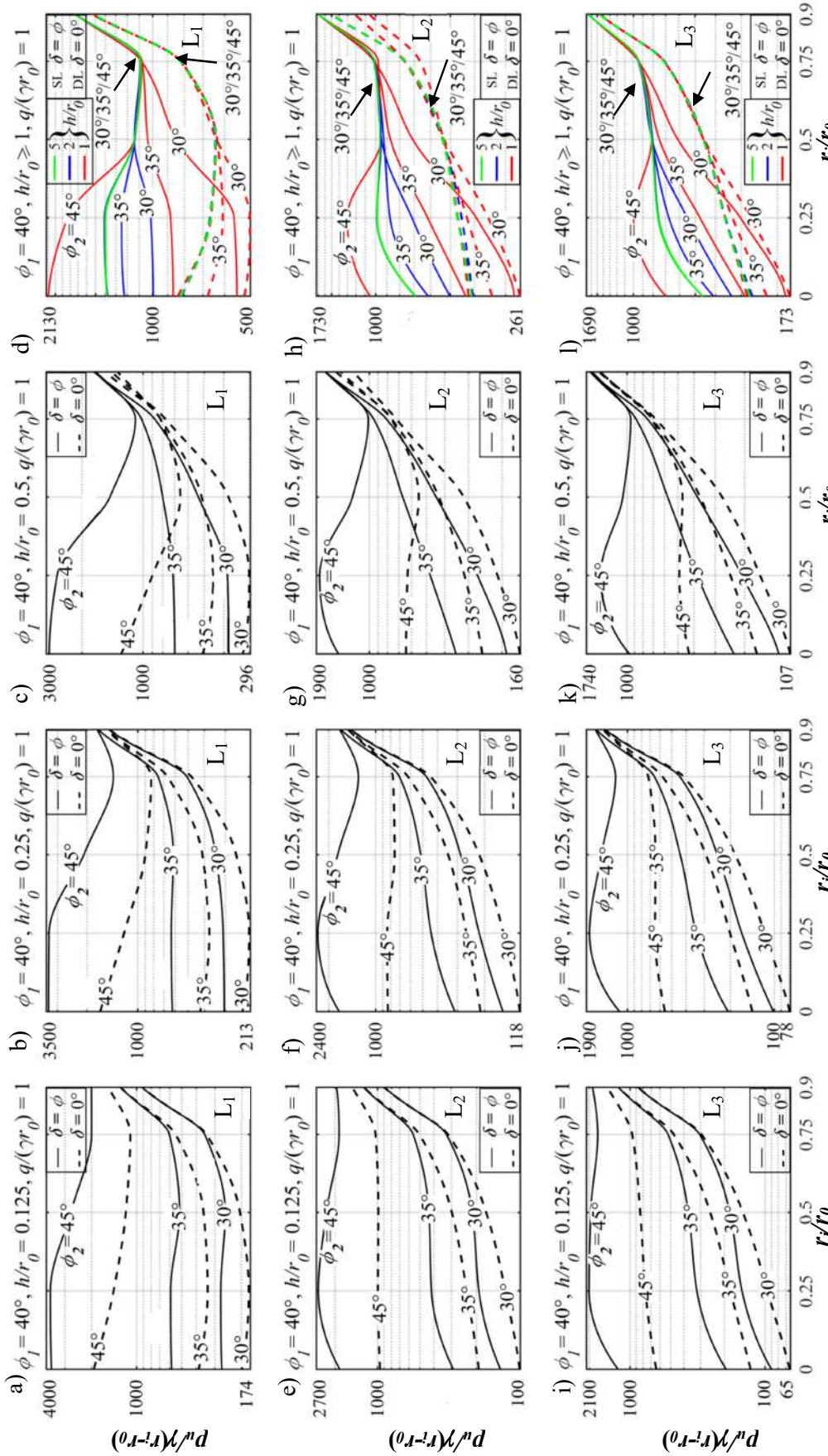

Figure 5.8 The variations of normalized bearing capacity with respect to r_i/r_0 for smooth and rough ring footing resting on a sand layer having ϕ_1=40° and different values of ϕ_2 with $q/(\gamma r_0)$=1 and corresponding to three different loading positions: (a–d) L_1; (e–h) L_2; and (i–l) L_3. SL: solid line; and DL: dashed line.

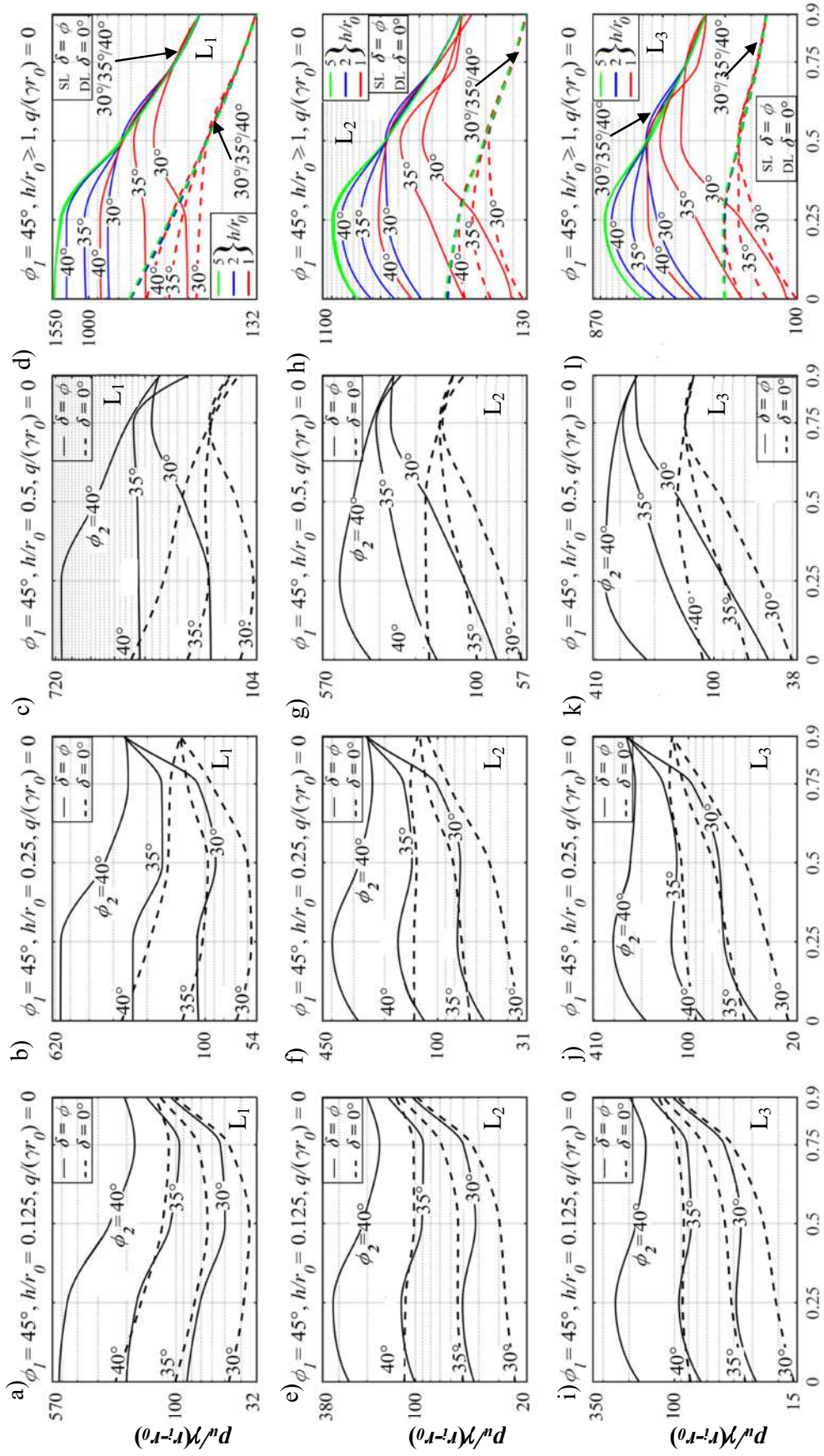

Figure 5.9 The variations of normalized bearing capacity with respect to r_i/r_0 for smooth and rough ring footing resting on a sand layer having ϕ_1=45° and different values of ϕ_2 with $q/(\gamma r_0)$=0 and corresponding to three different loading positions: (a–d) L_1; (e–h) L_2; and (i–l) L_3. SL: solid line; and DL: dashed line.

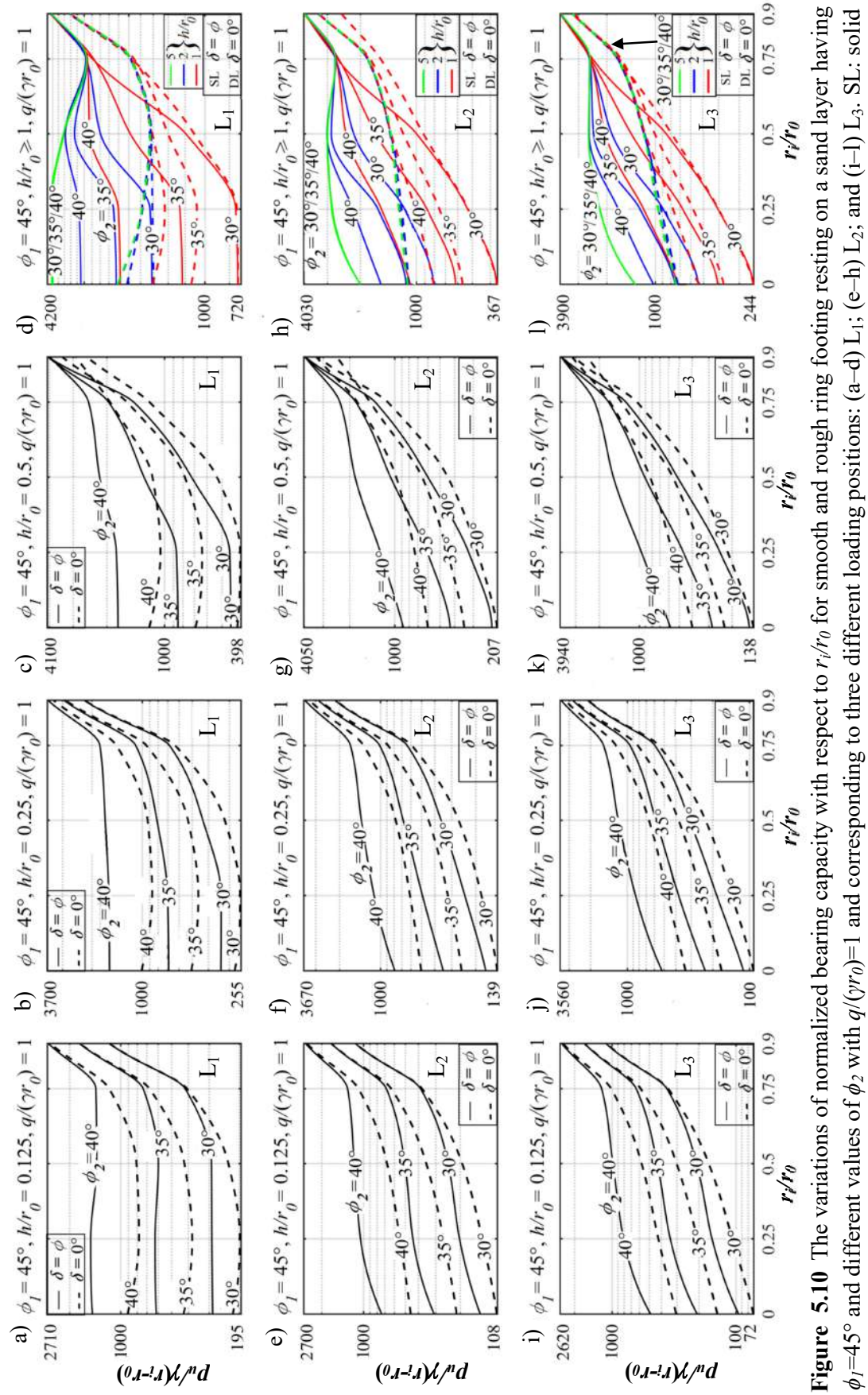

Figure 5.10 The variations of normalized bearing capacity with respect to r_i/r_0 for smooth and rough ring footing resting on a sand layer having ϕ_1=45° and different values of ϕ_2 with $q/(\gamma r_0)$=1 and corresponding to three different loading positions: (a–d) L_1; (e–h) L_2; and (i–l) L_3. SL: solid line; and DL: dashed line.

loading even if the surcharge pressure is taken into account. Although there is an appreciable difference between the numerical magnitudes, the nature of the p_u curves appear to be exactly similar for L_2 and L_3 loading conditions. It is further observed that in the absence of surcharge pressure, the difference of the p_u curves generated from the smooth and the rough foundations appears to be intact; on the contrary, the application of the surcharge pressure significantly reduces this difference as the width of the annular section reduces. Another way of representing the inclusion of the top layer between the ring foundation and the bottom layer is the non-dimensional efficiency factor, which is designated here with the symbol η; here, η is defined as the ratio of the

Table 5.2. The variation of efficiency factor (η) for ring footing resting on layered sands ($\phi_1 = 35°$ and $\phi_2 = 40°$) and corresponding to various loading positions, r_i/r_0 and h/r_0.

Loading position	r_i/r_0	h/r_0						
		0	0.125	0.25	0.5	1	2	5
L_0	0	1.000	0.853	0.748	0.589	0.391	0.341	0.34
	0.25	1.000	0.683	0.511	0.368	0.301	0.303	0.281
	0.50	1.000	0.636	0.448	0.333	0.335	0.328	0.334
	0.75	1.000	0.503	0.378	0.377	0.377	0.378	0.380
	0.90	1.000	0.404	0.408	0.407	0.405	0.405	0.404
L_1	0	1.000	0.851	0.748	0.589	0.391	0.346	0.346
	0.25	1.000	0.688	0.512	0.367	0.301	0.296	0.299
	0.50	1.000	0.634	0.447	0.331	0.333	0.333	0.332
	0.75	1.000	0.512	0.384	0.382	0.383	0.381	0.384
	0.90	1.000	0.404	0.406	0.408	0.406	0.406	0.407
L_2	0	1.000	0.851	0.752	0.588	0.390	0.347	0.349
	0.25	1.000	0.688	0.508	0.370	0.300	0.292	0.286
	0.50	1.000	0.638	0.453	0.333	0.297	0.334	0.334
	0.75	1.000	0.522	0.387	0.386	0.389	0.387	0.387
	0.90	1.000	0.407	0.401	0.407	0.407	0.407	0.406
L_3	0	1.000	0.855	0.750	0.590	0.391	0.349	0.349
	0.25	1.000	0.686	0.511	0.367	0.301	0.302	0.294
	0.50	1.000	0.629	0.444	0.333	0.331	0.334	0.334
	0.75	1.000	0.500	0.380	0.379	0.381	0.379	0.380
	0.90	1.000	0.404	0.404	0.404	0.403	0.404	0.404

bearing capacity of ring footing in the presence of the upper layer to the bearing capacity of ring footing placed only over the homogenous bottom layer. Table 5.2 lists the variation of η with respect to r_i/r_0, corresponding to different loading positions and various upper layer thickness of Type A1 soil having $\phi_1 = 35°$ and $\phi_2 = 40°$. It can be seen that the efficiency factor decreases with the radius ratio, but interestingly, it appears to be the same regardless of the loading positions. This can be inferred as the non-dependency of the efficiency factor on the position of loading application. Figures 5.11–5.14 represent the graphs between η versus h/r_0 for two different radius ratios considering with and without surcharging. The results are shown for smooth as well as rough ring footings. The value of η is either lower (for Type A1 soil) or greater (for Type A2 soil) than unity. The application of surcharge pressure seems to suppress the development of η for Type A2 soil. However, regardless of the loading positions, soil types, soil footing interface conditions, surcharge pressures, radius ratios, the value of η varies with h/r_0 up to a certain top layer thickness, beyond which η becomes almost constant. This can be attributed to the fact that after a certain value of h/r_0, the magnitude of p_u is not affected by the strength of the bottom layer. This specific thickness of the top sandy layer is termed here as optimum thickness (h_{opt}). Table 5.3 lists the variation of h_{opt}/r_0 with respect to different values of ϕ_1, ϕ_2, r_i/r_0, and $q/(\gamma r_0)$. The optimum thickness (h_{opt}) decreases as the strength of the bottom layer and radius ratio (r_i/r_0) increases, whereas it increases with the increase in the strength of the upper layer and the surcharge pressure. The optimum thickness (h_{opt}) is found to be smaller for smooth ring footing in comparison with its rough counterpart. Similar to η, h_{opt} also remains independent of the loading positions. It is also noteworthy, that there are few cases, especially for Type A2 soil with lower radius ratio, where the magnitude of η is higher for the smooth footing than the rough one.

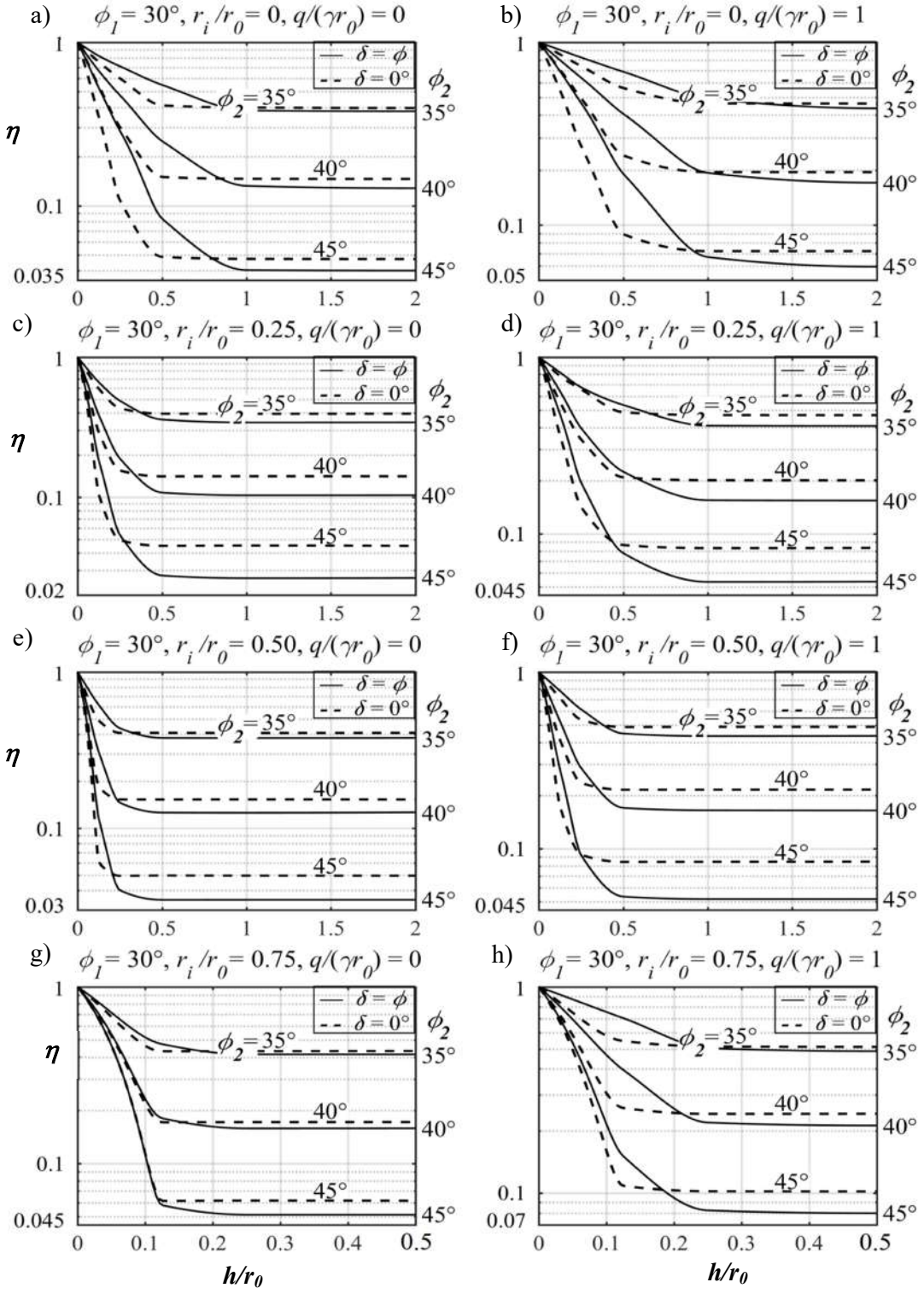

Figure 5.11 The variation of η with respect to h/r_0 for ring footing resting on layered sands (ϕ_1=30°) corresponding to with and without surcharge and four different radius ratios: (a and e) r_i/r_0=0; (b and f) r_i/r_0=0.25; (c and g) r_i/r_0=0.50; and (d and h) r_i/r_0=0.75.

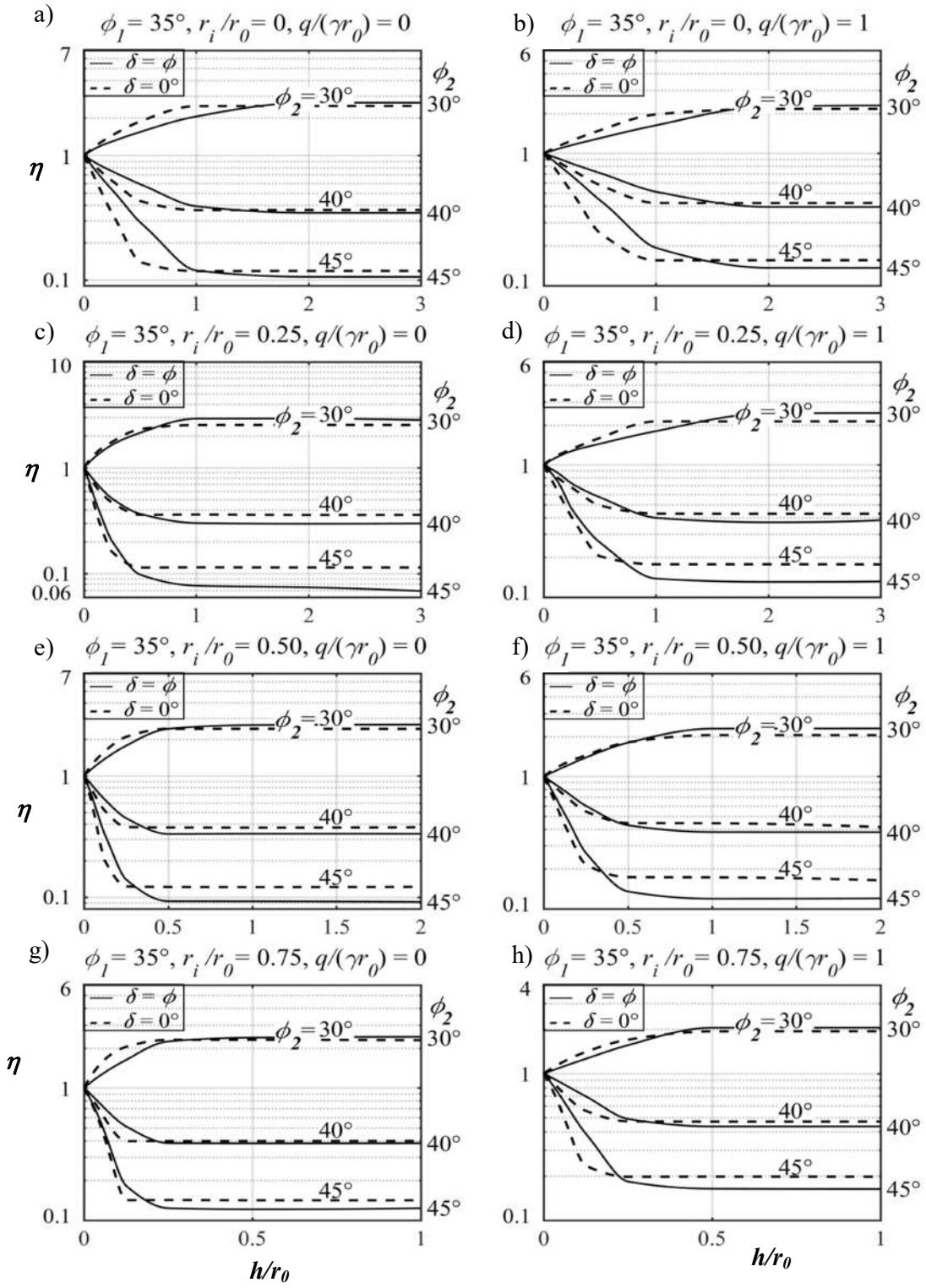

Figure 5.12 The variation of η with respect to h/r_0 for ring footing resting on layered sands (ϕ_1=35°) corresponding to with and without surcharge and four different radius ratios: (a and e) r_i/r_0=0; (b and f) r_i/r_0=0.25; (c and g) r_i/r_0=0.50; and (d and h) r_i/r_0=0.75.

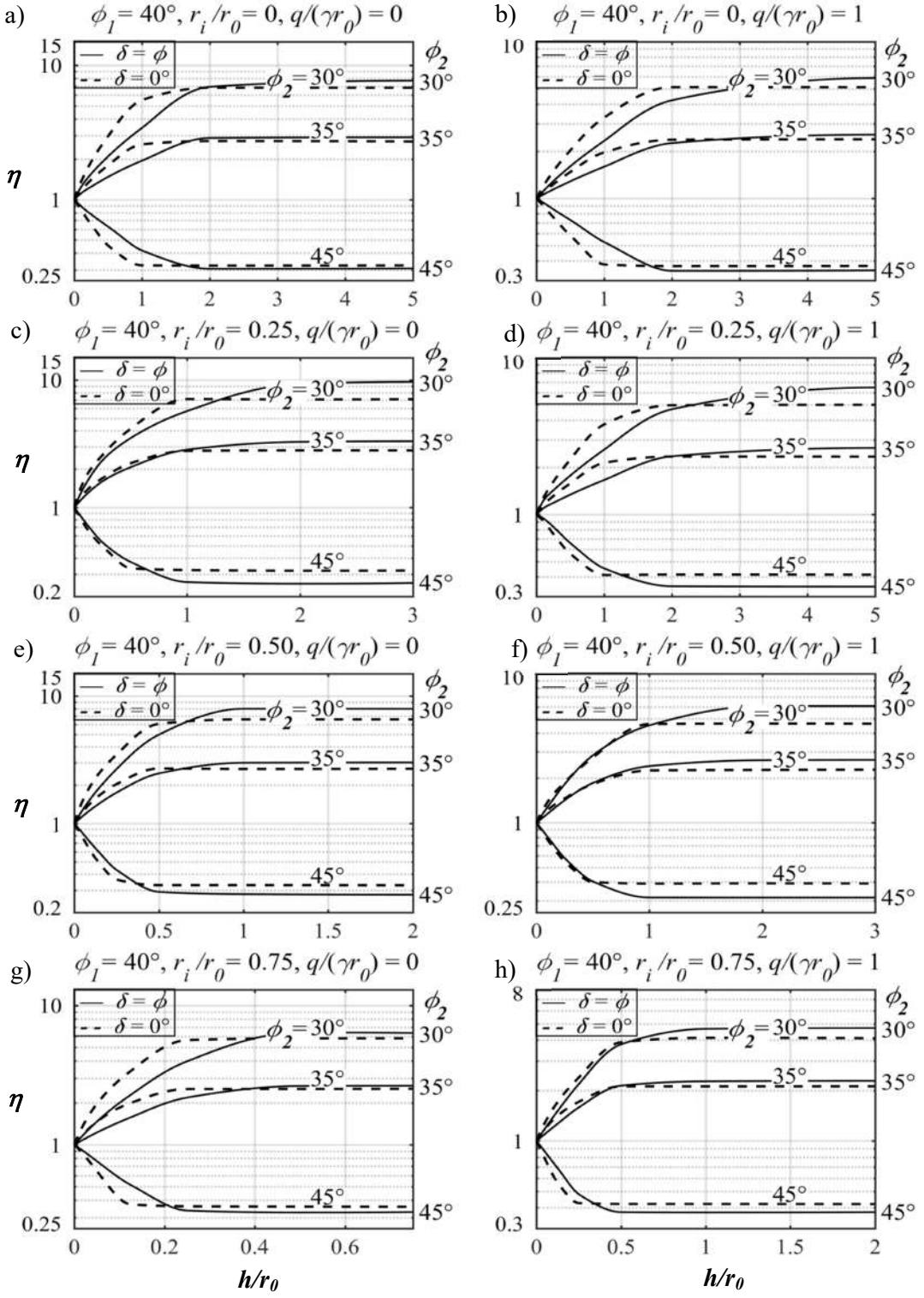

Figure 5.13 The variation of η with respect to h/r_0 for ring footing resting on layered sands (ϕ_1=40°) corresponding to with and without surcharge and four different radius ratios: (a and e) r_i/r_0=0; (b and f) r_i/r_0=0.25; (c and g) r_i/r_0=0.50; and (d and h) r_i/r_0=0.75.

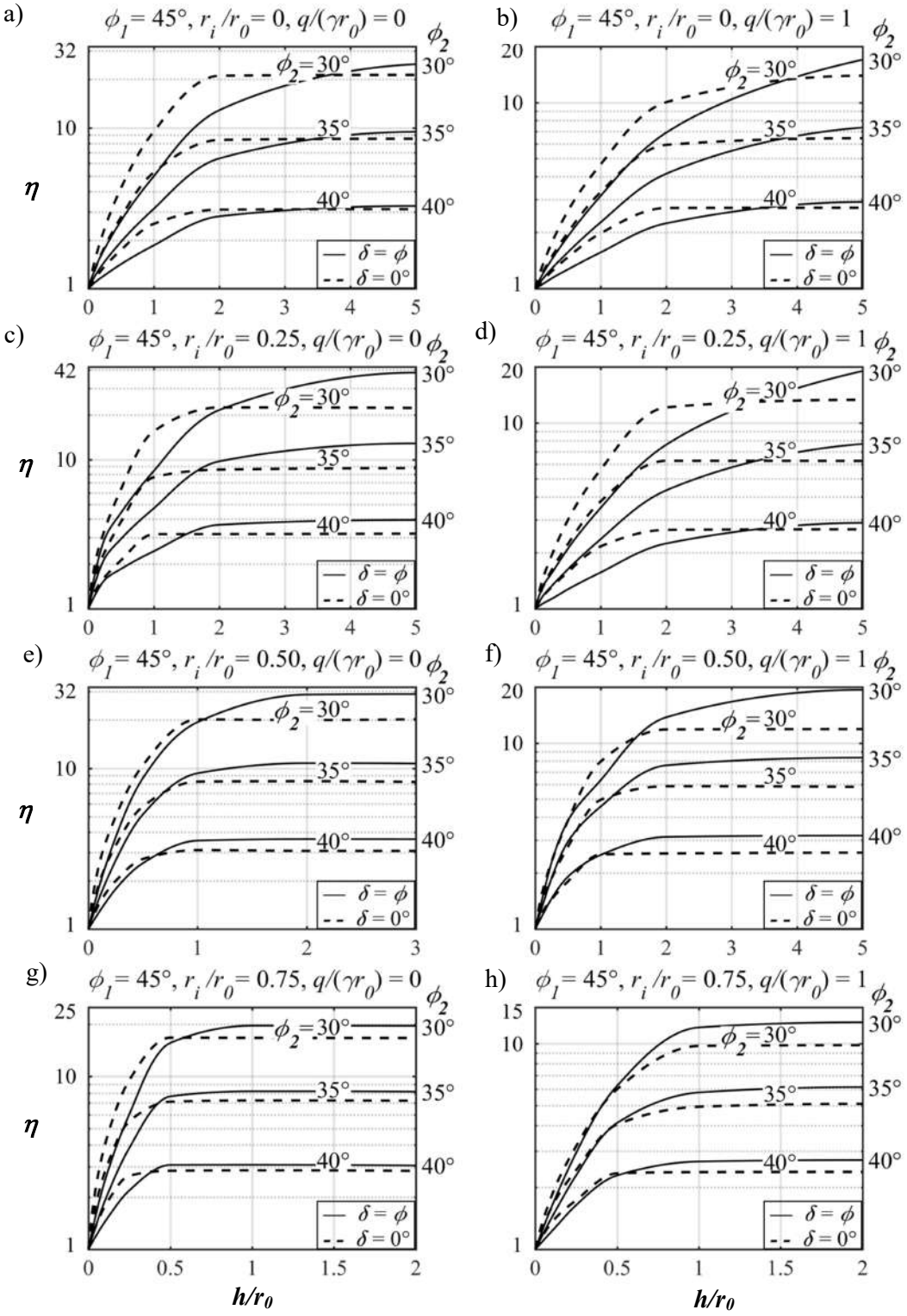

Figure 5.14 The variation of η with respect to h/r_0 for ring footing resting on layered sands ($\phi_1 = 45°$) corresponding to with and without surcharge and four different radius ratios: (a and e) r_i/r_0=0; (b and f) r_i/r_0=0.25; (c and g) r_i/r_0=0.50; and (d and h) r_i/r_0=0.75.

Table 5.3. The variation of h_{opt}/r_0 corresponding to different values of ϕ_1, ϕ_2, r_i/r_0, and $q/(\gamma r_0)$.

ϕ_1	r_i/r_0	h_{opt}/r_0							
		ϕ_2=30°		ϕ_2=35°		ϕ_2=40°		ϕ_2=45°	
		$q/(\gamma r_0)$ = 0.0	1.0	$q/(\gamma r_0)$ = 0.0	1.0	$q/(\gamma r_0)$ = 0.0	1.0	$q/(\gamma r_0)$ = 0.0	1.0
30º	0.00	--	--	1.40 (0.90)	1.60 (1.00)	1.20 (0.80)	1.30 (1.00)	1.00 (0.50)	1.10 (0.80)
	0.25	--	--	0.75 (0.45)	1.10 (0.60)	0.53 (0.47)	1.00 (0.55)	0.50 (0.37)	0.75 (0.40)
	0.50	--	--	0.60 (0.30)	0.70 (0.40)	0.40 (0.25)	0.50 (0.40)	0.40 (0.20)	0.50 (0.33)
	0.75	--	--	0.50 (0.19)	0.50 (0.25)	0.17 (0.14)	0.35 (0.14)	0.20 (0.13)	0.30 (0.15)
	0.90	--	--	0.20 (0.10)	0.30 (0.12)	0.12 (0.08)	0.12 (0.10)	0.10 (0.07)	0.10 (0.05)
35º	0.00	2.25 (1.20)	2.50 (2.00)	--	--	1.25 (1.00)	1.50 (1.30)	1.20 (0.60)	1.40 (1.10)
	0.25	1.50 (1.00)	1.73 (1.20)	--	--	1.00 (1.00)	1.20 (0.80)	0.70 (0.40)	1.00 (0.60)
	0.50	1.23 (0.67)	1.50 (0.80)	--	--	0.85 (0.65)	1.00 (0.75)	0.50 (0.35)	0.85 (0.40)
	0.75	0.75 (0.40)	0.80 (0.50)	--	--	0.60 (0.30)	0.70 (0.45)	0.30 (0.25)	0.50 (0.30)
	0.90	0.42 (0.25)	0.50 (0.30)	--	--	0.25 (0.20)	0.40 (0.25)	0.25 (0.25)	0.30 (0.2.0)
40º	0.00	7.50 (3.00)	10.00 (6.00)	3.00 (2.10)	7.00 (5.00)	--	--	2.30 (1.25)	2.50 (1.50)
	0.25	3.20 (2.00)	5.50 (5.00)	2.50 (1.25)	5.30 (2.50)	--	--	1.30 (1.00)	1.50 (1.00)
	0.50	2.40 (1.20)	3.00 (2.00)	1.75 (1.00)	2.50 (1.30)	--	--	0.90 (0.50)	1.00 (0.60)
	0.75	1.90 (0.70)	2.50 (1.50)	1.00 (0.80)	2.00 (1.10)	--	--	0.60 (0.30)	0.75 (0.35)
	0.90	0.60 (0.50)	1.00 (0.75)	0.75 (0.45)	1.00 (0.70)	--	--	0.25 (0.20)	0.25 (0.25)
45º	0.00	9.00 (5.00)	15.00 (10.00)	8.40 (3.00)	10.0 (9.00)	7.50 (2.70)	8.00 (5.00)	--	--
	0.25	7.80 (3.2)	9.50 (6.00)	7.00 (2.50)	8.00 (5.00)	5.00 (2.00)	7.00 (3.50)	--	--
	0.50	3.00 (1.60)	7.50 (3.50)	2.75 (1.40)	6.00 (2.50)	2.30 (1.00)	5.00 (2.00)	--	--
	0.75	2.30 (1.00)	4.50 (2.00)	1.70 (0.90)	3.20 (1.50)	1.20 (0.60)	2.50 (1.00)	--	--
	0.90	1.5 (0.50)	2.30 (1.00)	1.25 (0.50)	2.00 (0.70)	0.94 (0.30)	1.20 (0.50)	--	--

Note: The values inside and outside the parenthesis correspond to smooth and rough footing, respectively.

5.3.2.2 Case 2: Clayey layer underlain by another clayey layer (C-C case)

This section elaborates the study on the UBC of the ring footing placed over two different types of layered clays: weak clays over stronger one (Type B1) or strong clays over weaker stratum (Type B2). Figures 5.15–5.18 present the variation of p_u with respect to r_i/r_0 corresponding to various loading positions, soil types, top layer thicknesses, and for two different surcharge loadings, namely, $q/(\gamma r_0)$ = 0 and 1. Irrespective of the soil type, the bearing capacity is found to be greater when the

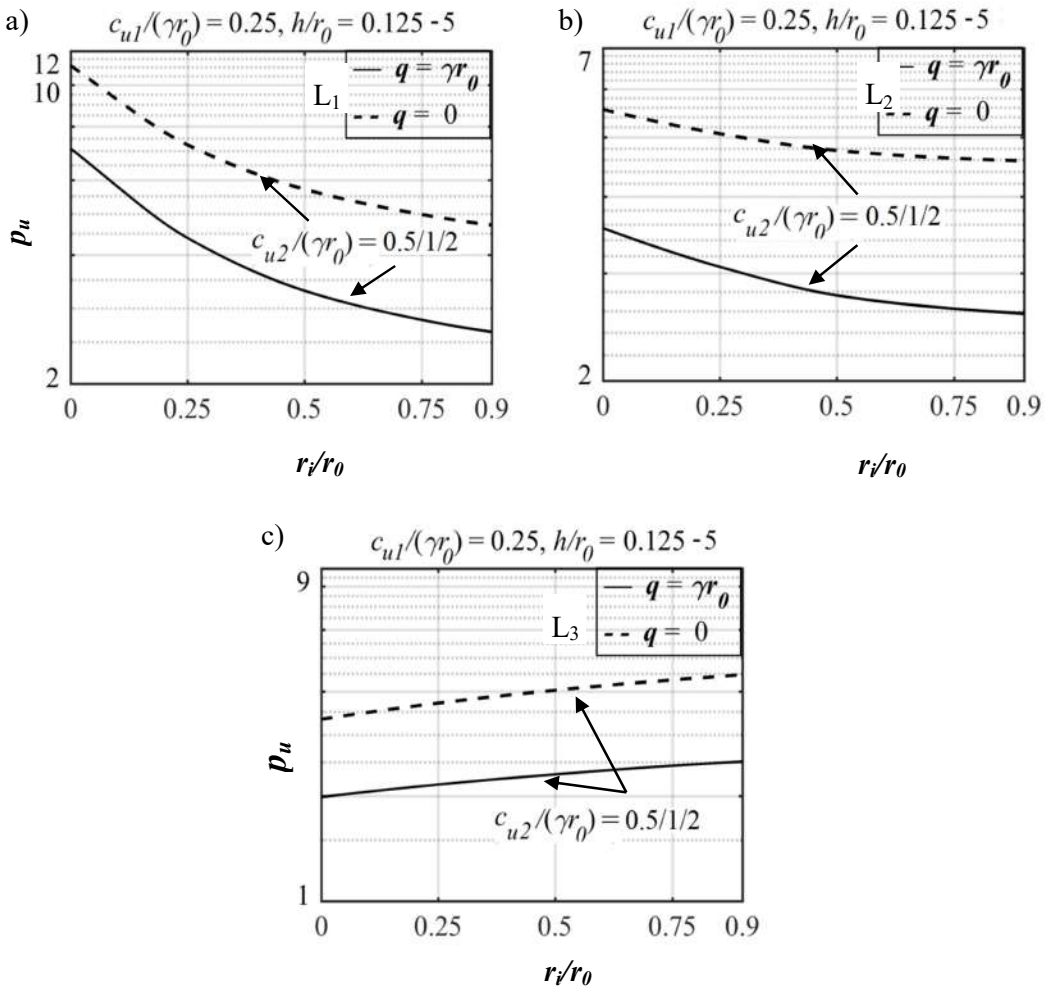

Figure 5.15 The variation of UBC with respect to r_i/r_0 for ring footing resting on clayey soil having cohesion ($c_{u1}/(\gamma r_0)$ = 0.25) overlying on clayey soils ($c_{u2}/(\gamma r_0)$) and corresponding to three different loading positions: a) L_1; b) L_2; c) L_3.

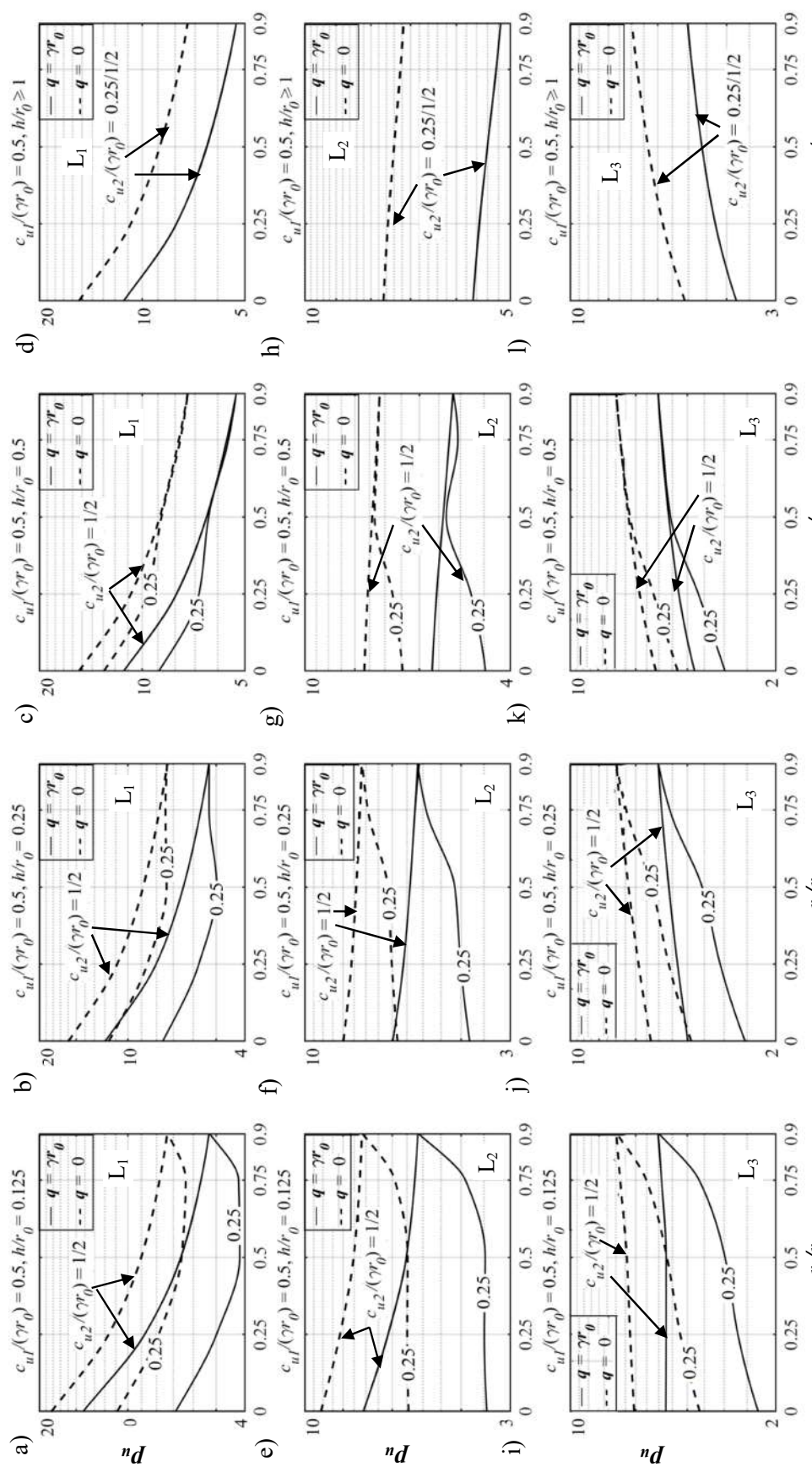

Figure 5.16 The variation of UBC with respect to r_i/r_0 for ring footing resting on clayey soil having cohesion ($c_{u1}/(\gamma r_0)$ =0.50) overlying on clayey soils ($c_{u2}/(\gamma r_0)$) and corresponding to three different loading positions: (a-d) L_1; (e-h) L_2; (i-l) L_3.

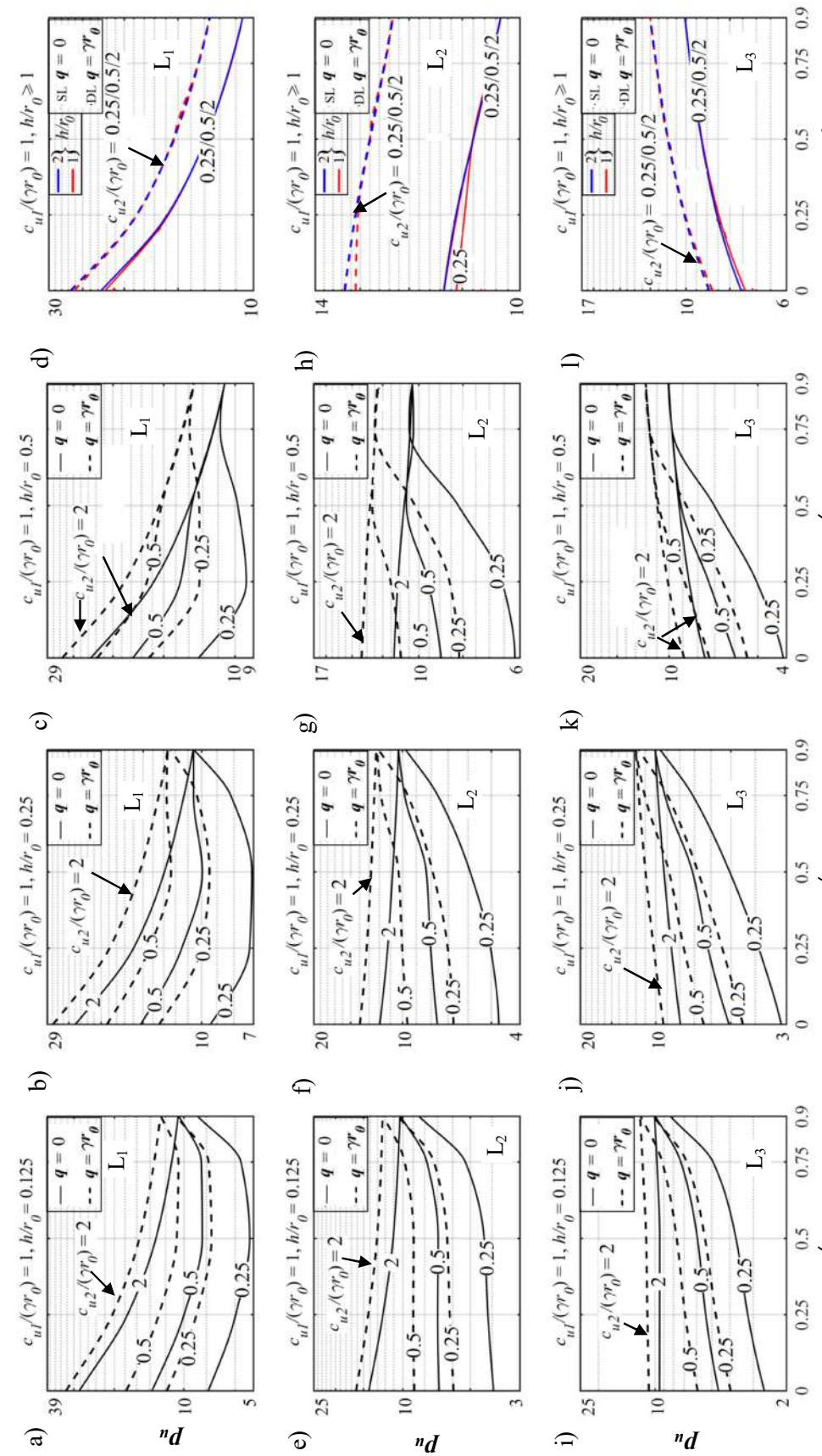

Figure 5.17 The variation of UBC with respect to r_i/r_0 for ring footing resting on clayey soil having cohesion ($c_{u1}/(\gamma r_0)$ =1.0) overlying on clayey soils ($c_{u2}/(\gamma r_0)$) and corresponding to three different loading positions: (a-d) L_1; (e-h) L_2; (i-l) L_3. SL: solid line; and DL: dashed line.

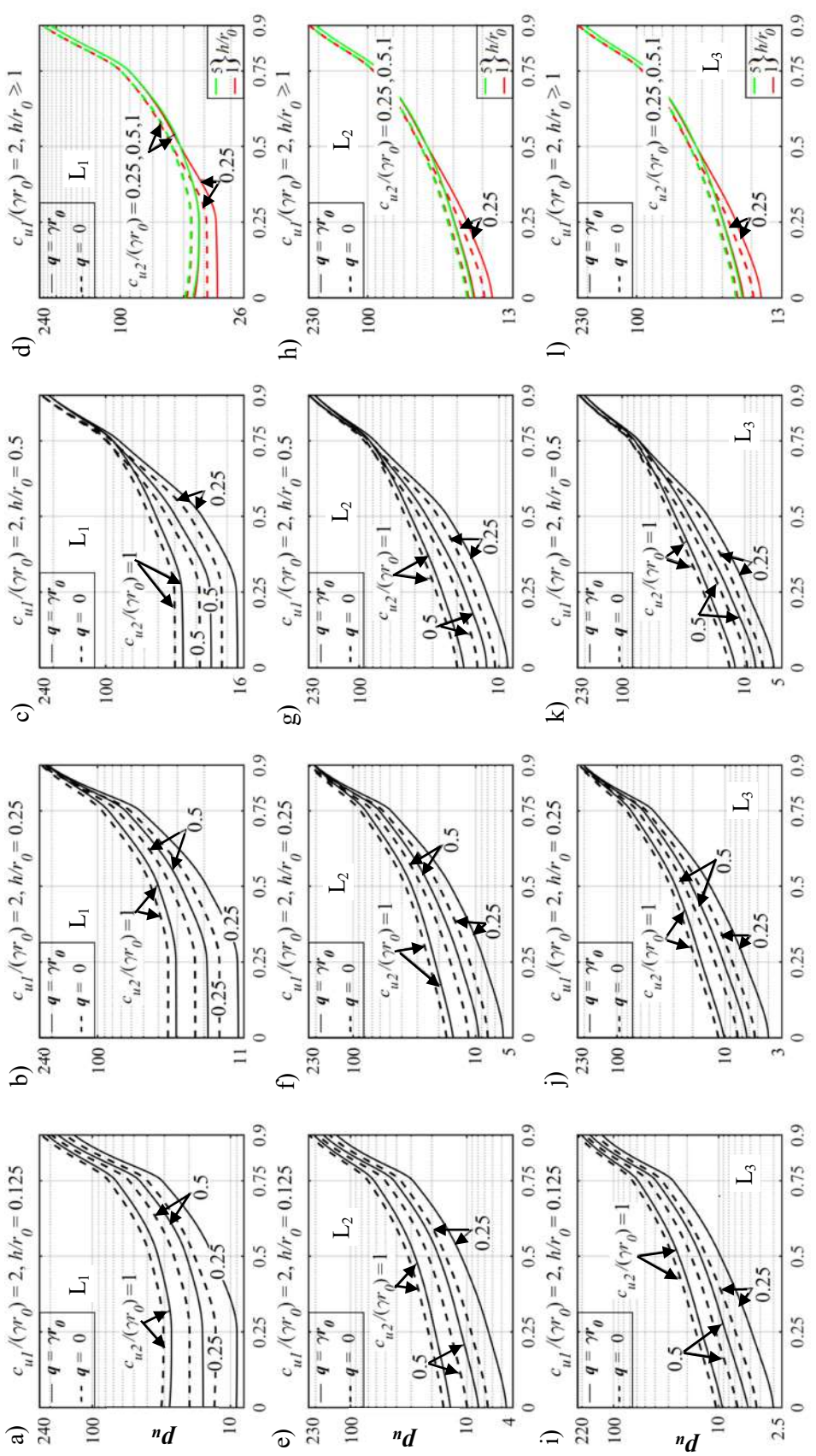

Figure 5.18 The variation of UBC with respect to r_i/r_0 for ring footing resting on clayey soil having cohesion ($c_{u1}/(\gamma r_0)$ =2.0) overlying on clayey soils ($c_{u2}/(\gamma r_0)$) and corresponding to three different loading positions: (a-d) L_1; (e-h) L_2; (i-l) L_3.

surcharge pressure is being applied; however, the deviations between the curves for $q/(\gamma r_0) = 0$ and 1 appear to be more significant for soil Type B2 and L_2 loading position but are not affected by the r_i/r_0 ratio. For soil Type B1, the undrained cohesive strength of the bottom layer and the thickness of the top layer hardly play any role in influencing the bearing capacity of the layered soil, whereas for soil Type B2, p_u increases with the increase in the undrained strength of the bottom layer. The nature of the p_u curves is distinctly associated with the type of loading conditions−the curves appear to be sharp decreasing, almost constant, and noticeably increasing for L_1, L_2, and L_3 loadings, respectively.

Figures 5.19−5.20 show the variation of η with h/r_0 for different soil strength and surcharge pressure. For soil Type B1, η remains smaller than unity, whereas for soil Type B2, $\eta > 1$. It should be noted that η remains unaltered with the loading positions. Nevertheless, similar to the layered sands, the existence of optimum thickness (h_{opt}) is quite prominent over here as well. Table 5.4 lists the variation of h_{opt}/r_0 corresponding to different values of $c_{u1}/(\gamma r_0)$, $c_{u2}/(\gamma r_0)$, r_i/r_0, and $q/(\gamma r_0)$. The optimum thickness (h_{opt}) decreases with increase in the strength of the bottom layer, surcharge pressure $q/(\gamma r_0)$, and radius ratio (r_i/r_0), whereas it increases with increase in the strength of upper layer.

5.3.2.3 Case 3: Sandy layer underlain by clayey layer (S-C case)

The results are presented in two different terms: absolute term (normalized bearing capacity) and relative comparison term (efficiency factor). Figures 5.21−5.28 present the normalized bearing capacity with respect to the radius ratio (r_i/r_0) corresponding to various values of $c_u/(\gamma r_0)$, ϕ, $q/\gamma r_0$, and h/r_0 and subjected to different loading positions. The continuous and dotted lines represent the UBC pertaining to rough and smooth footing, respectively. The effect of surcharge pressure is duly

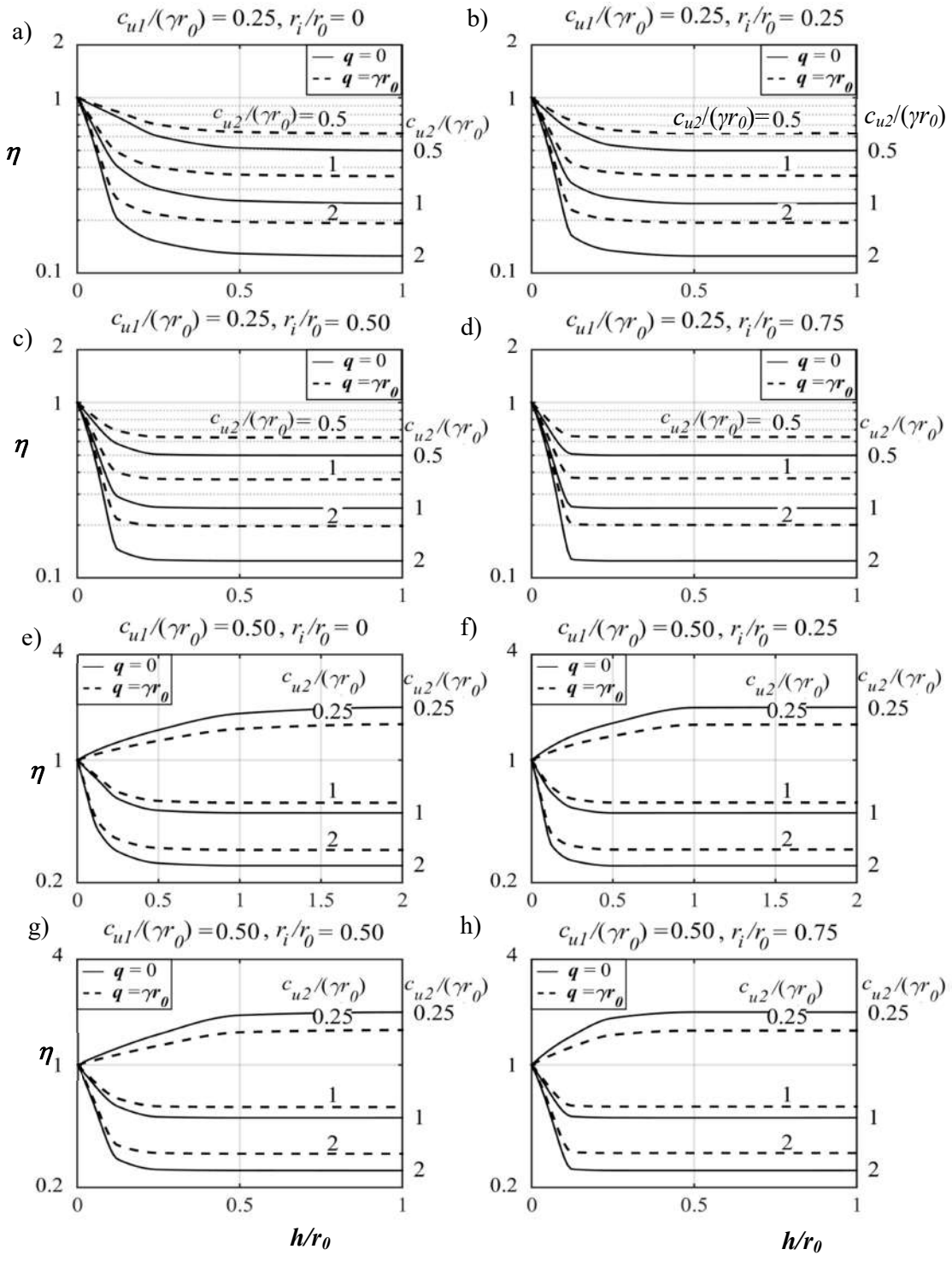

Figure 5.19 The variation of η with respect to h/r_0 for ring footing resting on layered clays corresponding to four different radius ratios: (a and e) r_i/r_0=0; (b and f) r_i/r_0=0.25; (c and g) r_i/r_0=0.50; and (d and h) r_i/r_0=0.75.

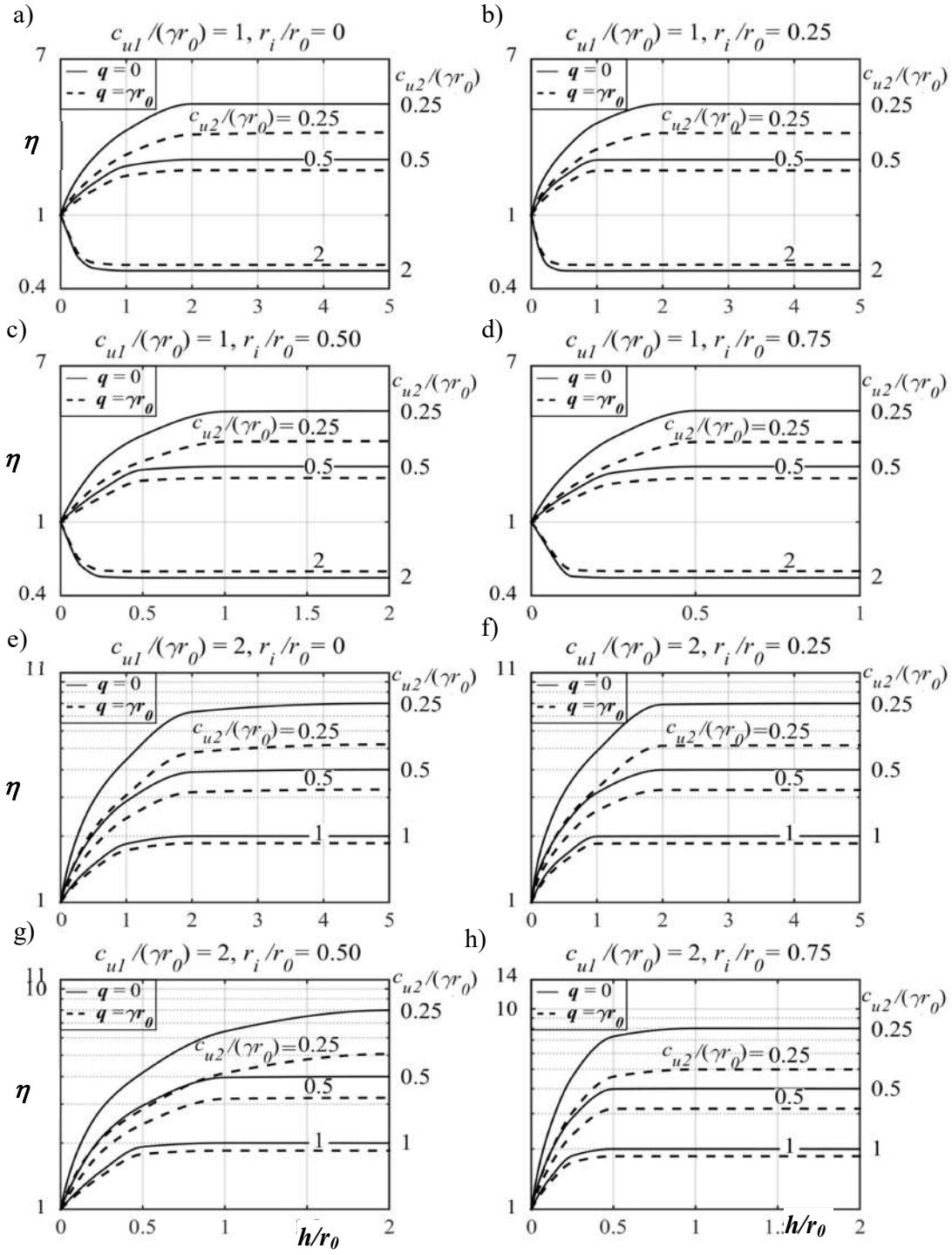

Figure 5.20 The variation of η with respect to h/r_0 for ring footing resting on layered clays corresponding to four different radius ratios: (a and e) r_i/r_0=0; (b and f) r_i/r_0=0.25; (c and g) r_i/r_0=0.50; and (d and h) r_i/r_0=0.75.

Table 5.4. The variation of h_{opt}/r_0 corresponding to different values of $c_{u1}/(\gamma r_0)$, $c_{u2}/(\gamma r_0)$, r_i/r_0, and $q/(\gamma r_0)$.

$c_{u1}/(\gamma r_0)$	r_i/r_0	h_{opt}/r_0							
		$c_{u2}/(\gamma r_0)$ =0.25		$c_{u2}/(\gamma r_0)$ =0.50		$c_{u2}/(\gamma r_0)$ =1.00		$c_{u2}/(\gamma r_0)$ =2.00	
		$q/(\gamma r_0)$ = 0.0	1.0	$q/(\gamma r_0)$ = 0.0	1.0	$q/(\gamma r_0)$ = 0.0	1.0	$q/(\gamma r_0)$ = 0.0	1.0
0.25	0.00	--	--	0.30	0.45	0.40	0.50	0.45	0.50
	0.25	--	--	0.25	0.30	0.35	0.50	0.30	0.25
	0.50	--	--	0.12	0.15	0.25	0.30	0.20	0.15
	0.75	--	--	0.10	0.10	0.15	0.20	0.10	0.12
	0.90	--	--	0.10	0.10	0.10	0.10	0.10	0.10
0.50	0.00	1.20	1.50	--	--	0.40	0.40	0.40	0.40
	0.25	0.90	1.00	--	--	0.30	0.30	0.30	3.00
	0.50	0.75	0.80	--	--	0.25	0.30	0.25	0.25
	0.75	0.50	0.60	--	--	0.20	0.25	0.12	0.12
	0.90	0.25	0.40	--	--	0.10	0.15	0.10	0.10
1.00	0.00	2.00	5.00	2.00	2.00	--	--	0.50	1.00
	0.25	2.00	2.00	2.00	2.00	--	--	0.50	0.50
	0.50	1.00	1.50	0.75	1.00	--	--	0.25	0.50
	0.75	0.50	1.00	0.50	0.50	--	--	0.12	0.25
	0.90	0.50	0.50	0.50	0.75	--	--	0.12	0.12
2.00	0.00	5.00	5.00	2.00	5.00	2.00	2.00	--	--
	0.25	2.00	5.00	2.00	2.00	1.00	1.00	--	--
	0.50	2.00	2.00	1.00	2.00	0.75	1.00	--	--
	0.75	1.00	1.00	0.50	0.50	0.50	0.50	--	--
	0.90	0.25	0.50	0.25	0.50	0.25	0.50	--	--

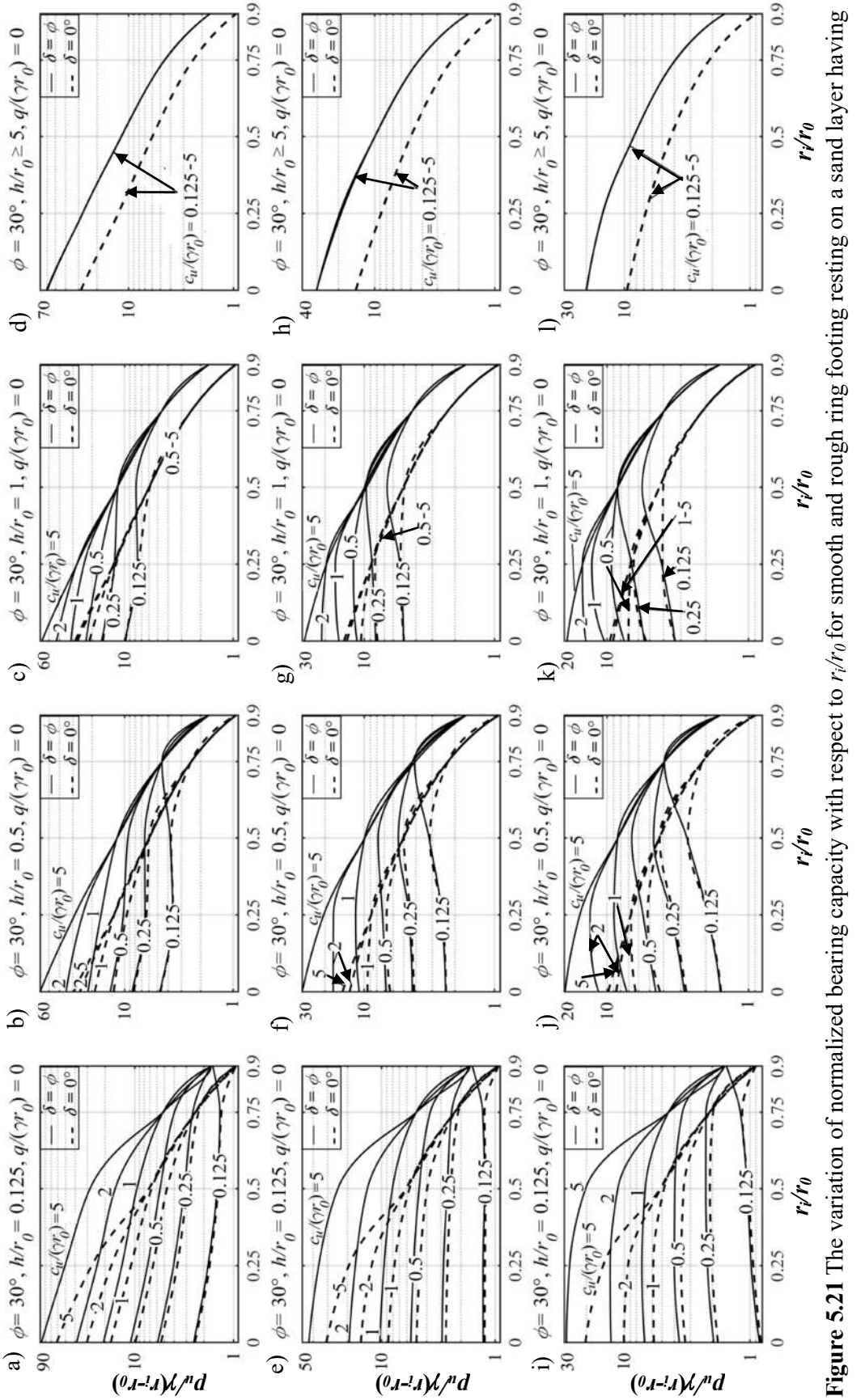

Figure 5.21 The variation of normalized bearing capacity with respect to r_i/r_0 for smooth and rough ring footing resting on a sand layer having ϕ =30° and different values of $c_u/(\gamma r_0)$ with $q/(\gamma r_0) = 0$ and corresponding to three different loading positions: (a-d) L_1; (e-h) L_2; and (i-l) L_3.

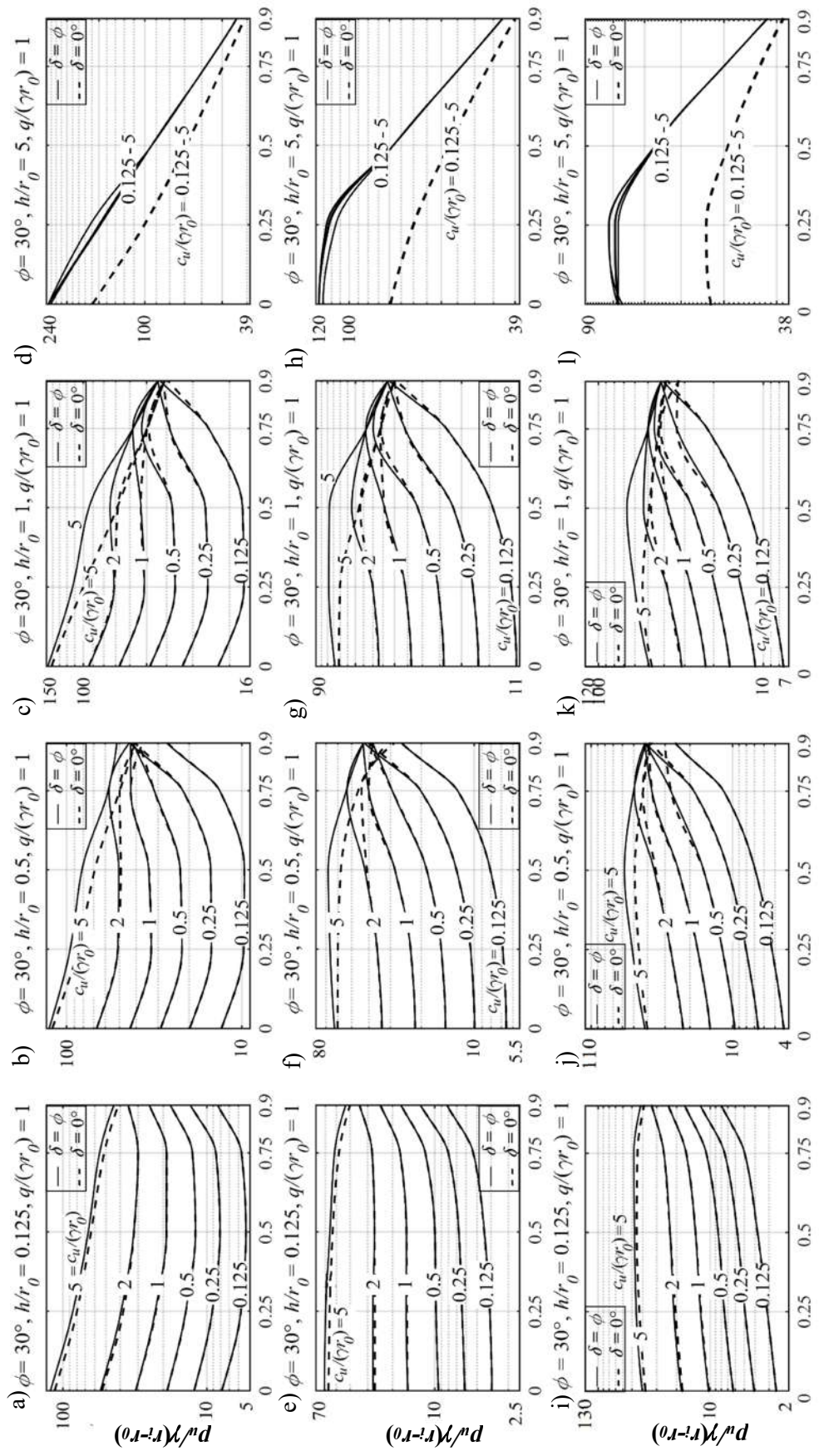

Figure 5.22 The variations of normalized bearing capacity with respect to r_i/r_0 for smooth and rough ring footing resting on a sand layer having ϕ =30° and different values of $c_u/(\gamma r_0)$ with $q/(\gamma r_0) = 1$ and corresponding to three different loading positions: (a-d) L_1; (e-h) L_2; and (i-l)

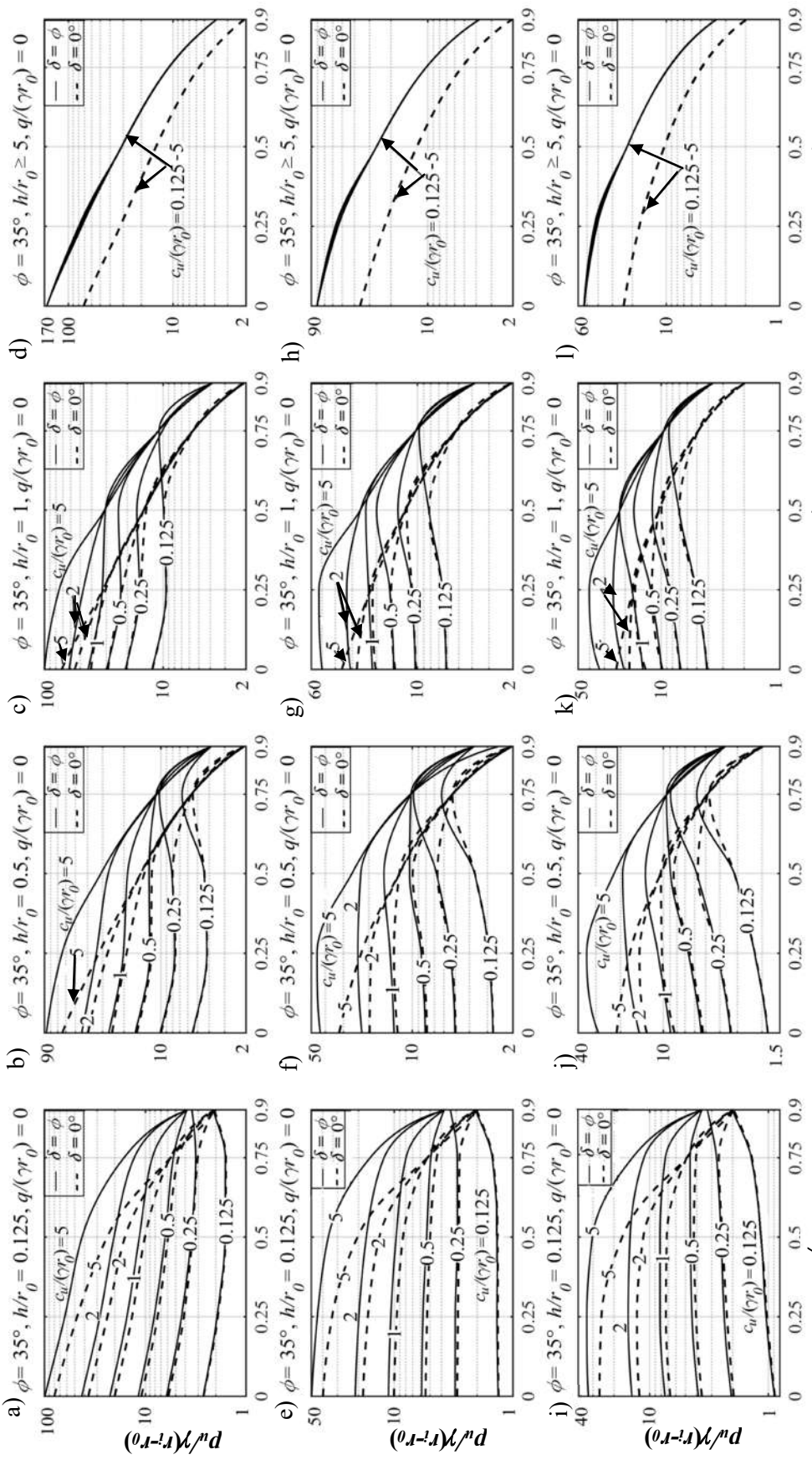

Figure 5.23 The variations of normalized bearing capacity with respect to r_i/r_0 for smooth and rough ring footing resting on a sand layer having ϕ =35° and different values of $c_u/(\gamma r_0)$ with $q/(\gamma r_0) = 0$ and corresponding to three different loading positions: (a-d) L_1; (e-h) L_2; and (i-l) L_3.

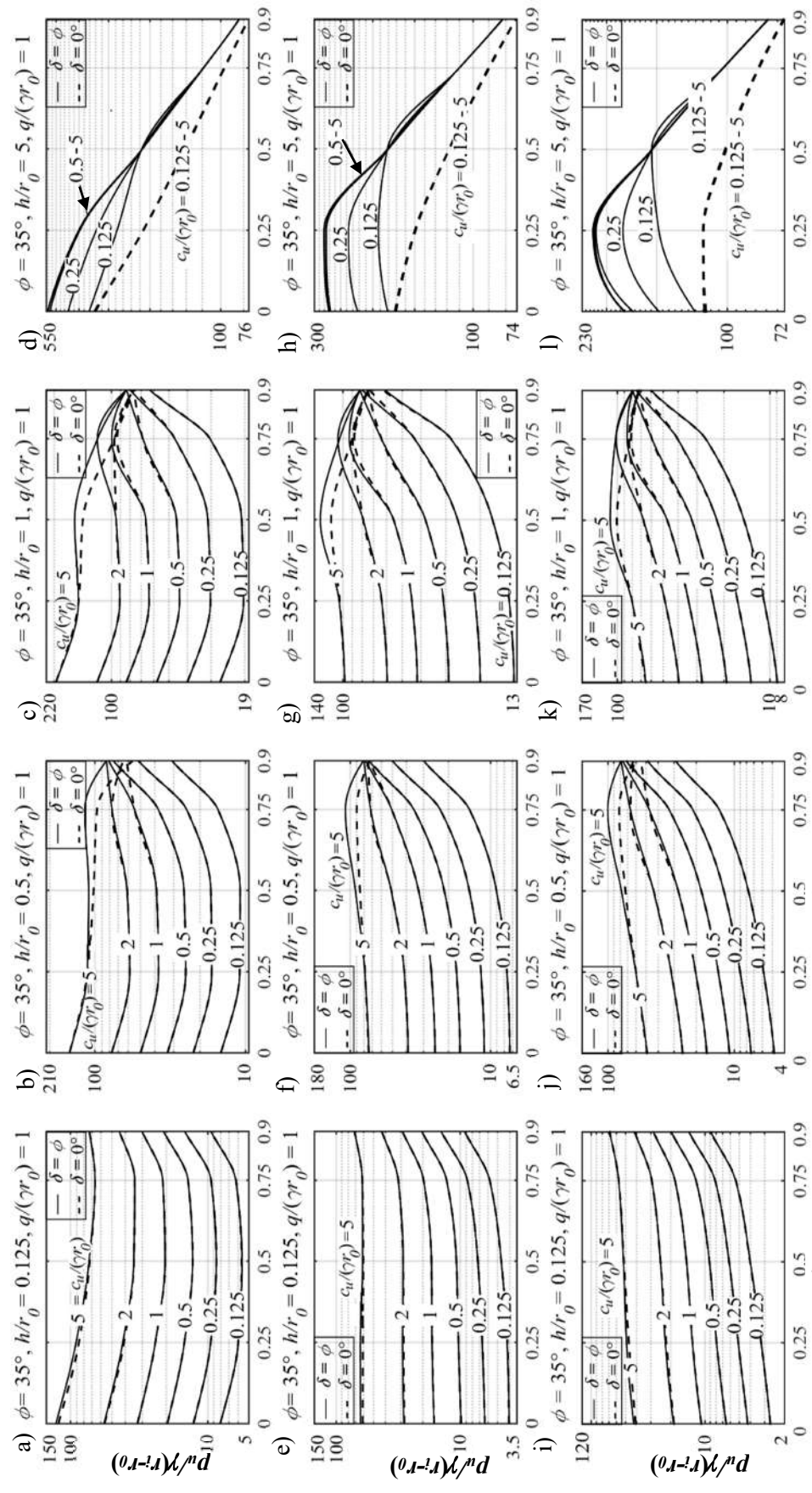

Figure 5.24 The variations of normalized bearing capacity with respect to r_i/r_0 for smooth and rough ring footing resting on a sand layer having ϕ =35° and different values of $c_u/(\gamma r_0)$ with $q/(\gamma r_0)$ = 1 and corresponding to three different loading positions: (a-d) L_1; (e-h) L_2; and (i-l) L_3.

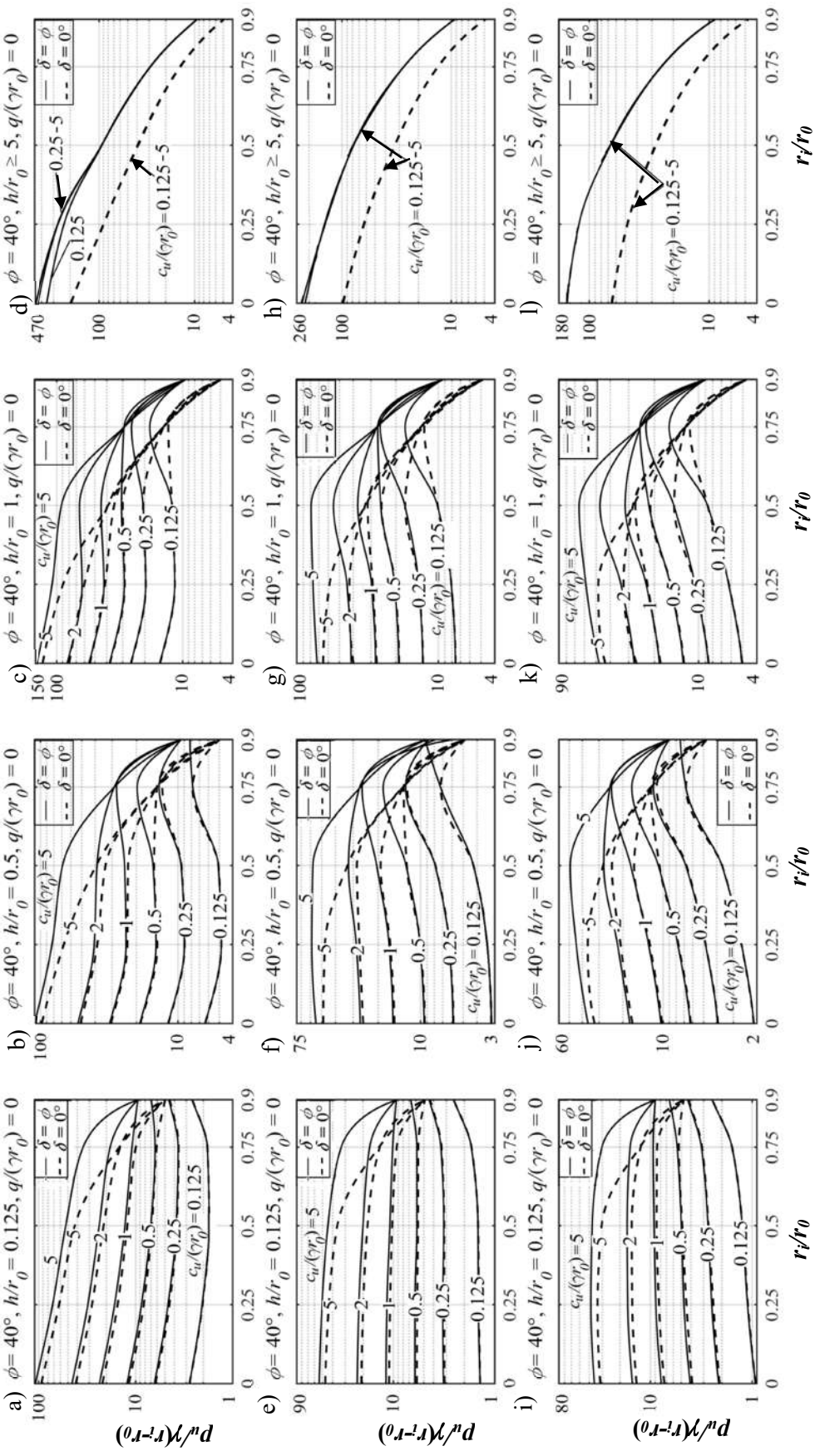

Figure 5.25 The variations of normalized bearing capacity with respect to r_i/r_0 for smooth and rough ring footing resting on a sand layer having ϕ =40° and different values of $c_u/(\gamma r_0)$ with $q/(\gamma r_0) = 0$ and corresponding to three different loading positions: (a-d) L_1; (e-h) L_2; and (i-l) L_3.

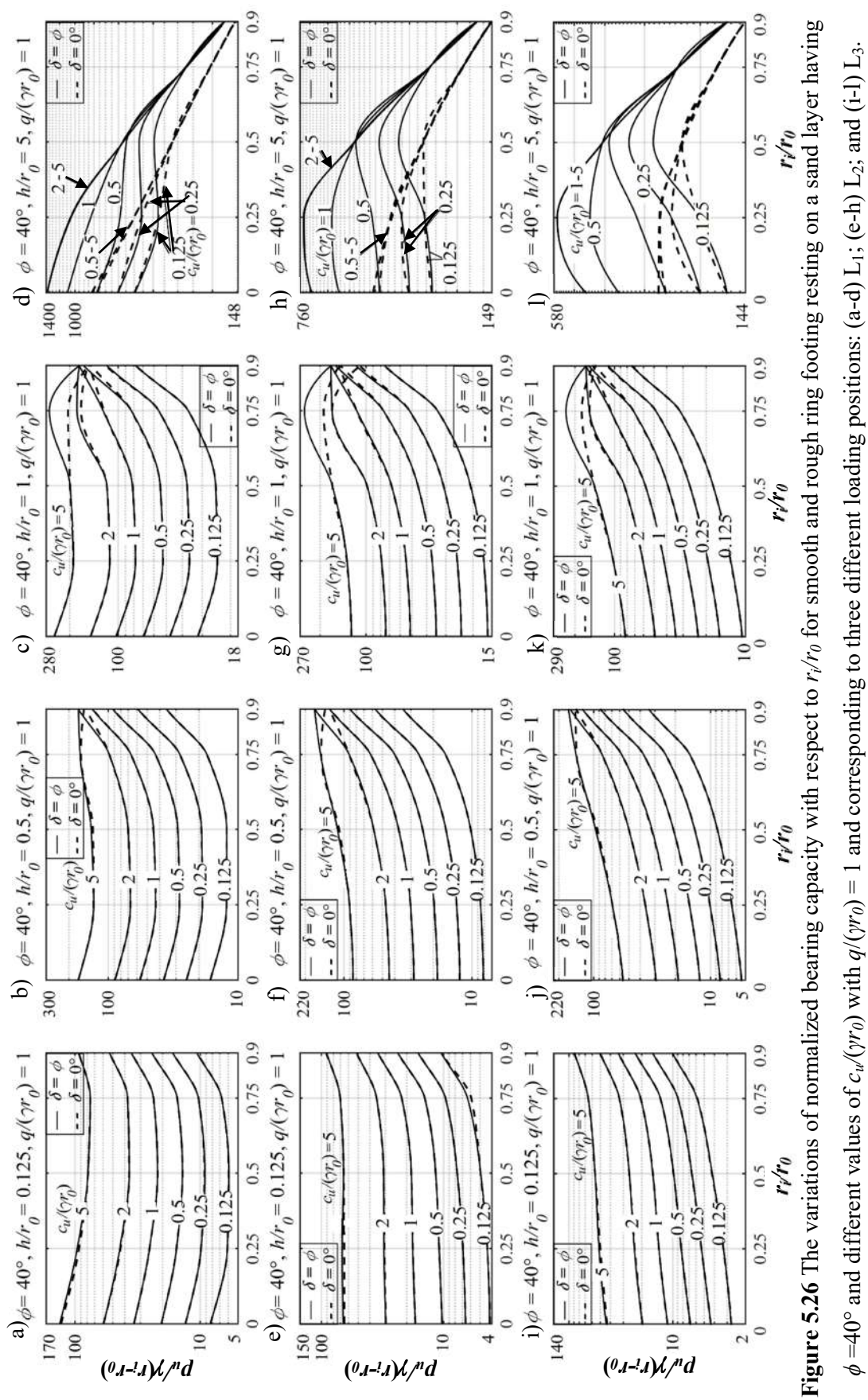

Figure 5.26 The variations of normalized bearing capacity with respect to r_i/r_0 for smooth and rough ring footing resting on a sand layer having ϕ =40° and different values of $c_u/(\gamma r_0)$ with $q/(\gamma r_0)$ = 1 and corresponding to three different loading positions: (a-d) L_1; (e-h) L_2; and (i-l) L_3.

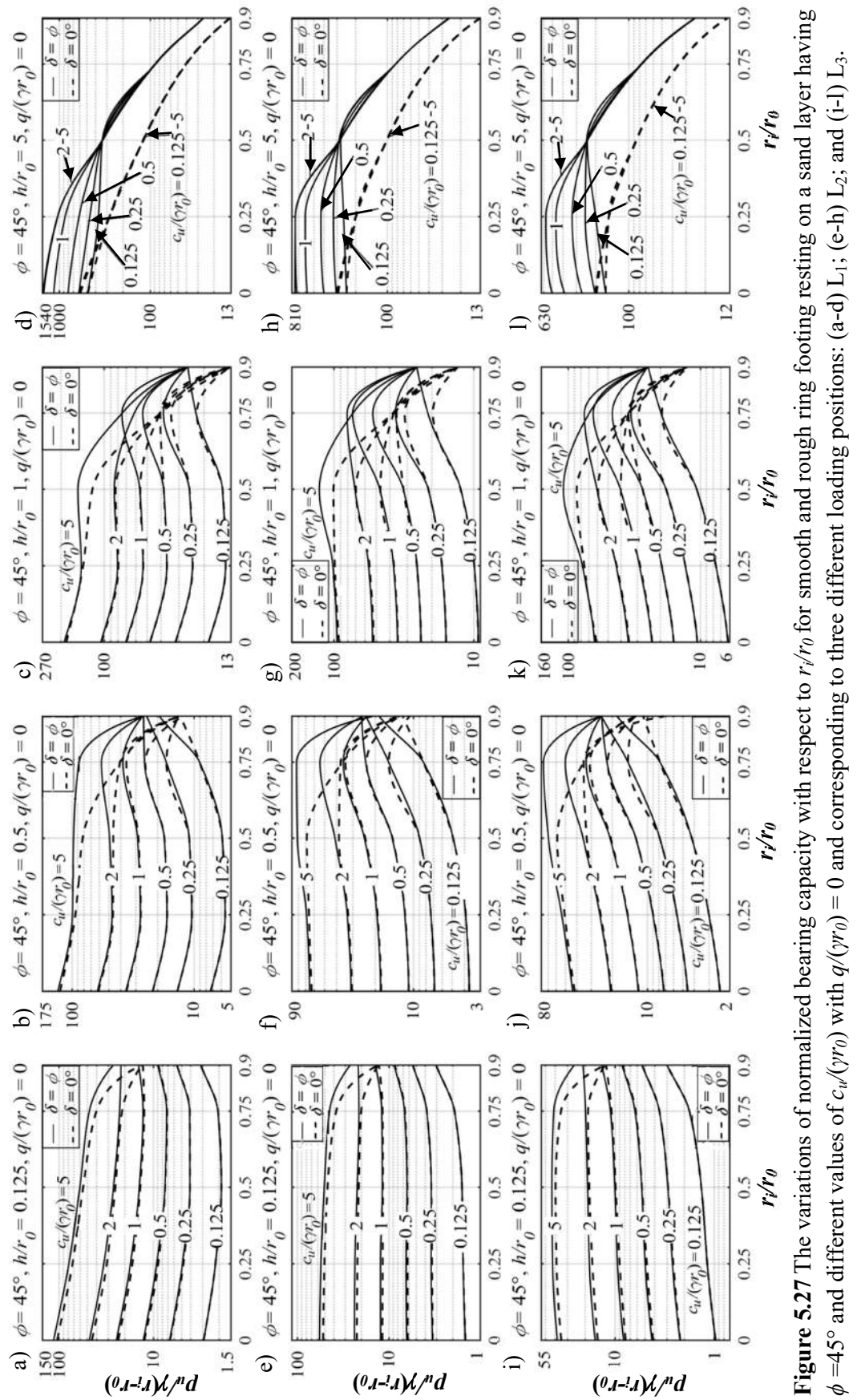

Figure 5.27 The variations of normalized bearing capacity with respect to r_i/r_0 for smooth and rough ring footing resting on a sand layer having ϕ =45° and different values of $c_u/(\gamma r_0)$ with $q/(\gamma r_0) = 0$ and corresponding to three different loading positions: (a-d) L_1; (e-h) L_2; and (i-l) L_3.

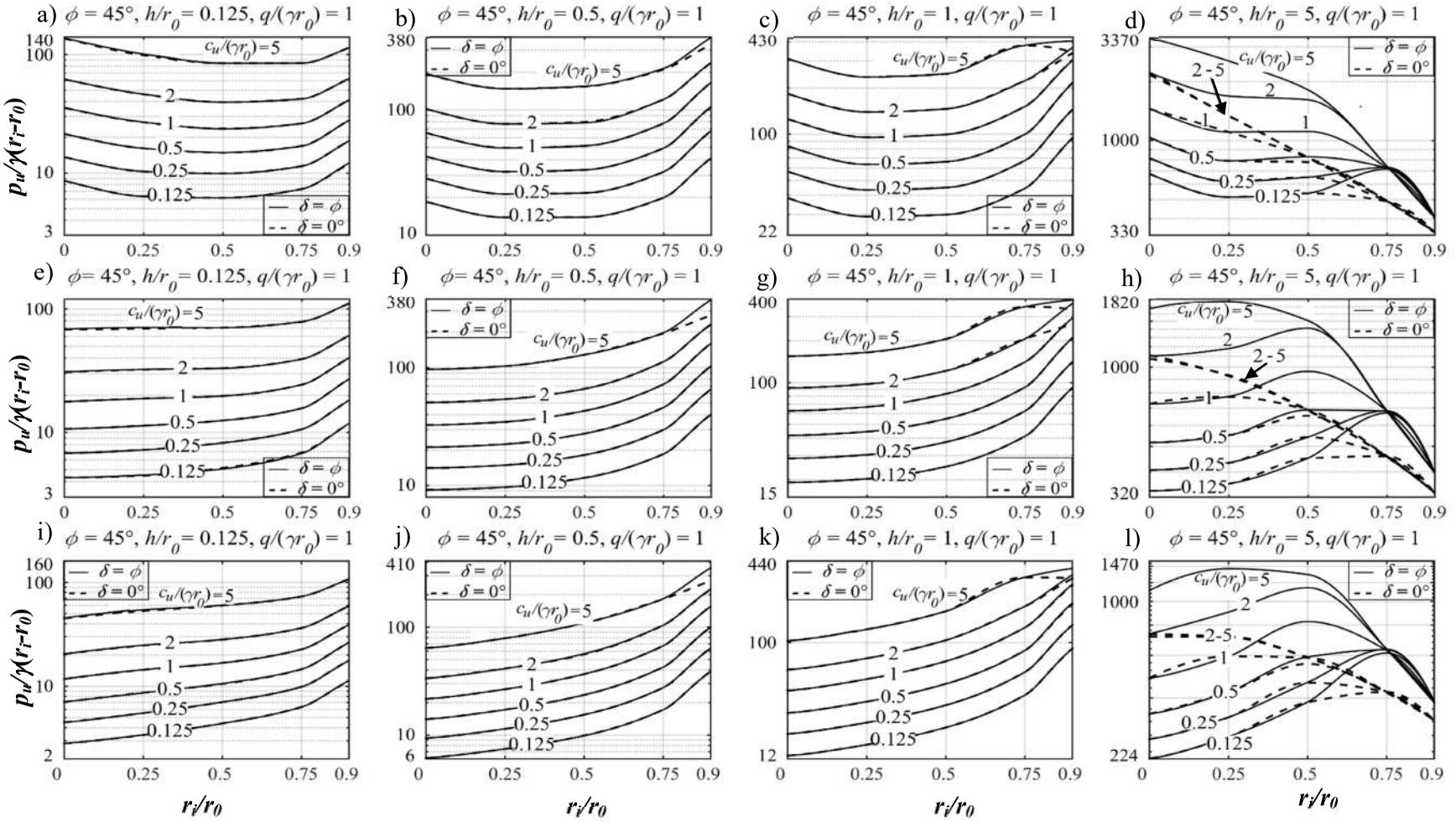

Figure 5.28 The variations of normalized bearing capacity with respect to r_i/r_0 for smooth and rough ring footing resting on a sand layer having ϕ =45° and different values of $c_u/(\gamma r_0)$ with $q/(\gamma r_0)$ = 1 and corresponding to three different loading positions: (a-d) L_1; (e-h) L_2; and (i-l) L_3.

examined. Figures 5.29–5.32 depict the variation of efficiency factor (η) with respect to the sand layer thickness. The following observations are noted:

a) Irrespective of the friction angle, surcharging effect, and footing roughness, the normalized bearing capacity of ring footing appears to be maximum for inner half loading (L_1) and minimum for outer half loading (L_3).

b) The variations in loading arrangement result in a notable discrepancy in the trend of the UBC curves too; especially, when the bottom clay layer is relatively weak and the inserted sand layer is having a very small thickness ($h/r_0 \leq 0.5$). For $\phi = 35°$ and $q = 0$, the UBC curves related to $c_u/(\gamma r_0) \leq 0.5$ either decrease or remains to be constant with r_i/r_0 when the loading is of L_1 type; nonetheless, if the loading is of L_3 type the UBC curves corresponding to $c_u/(\gamma r_0) \leq 0.5$ continuously increases with r_i/r_0. In the presence of surcharge pressure ($q = \gamma r_0$), the L_1-type loading generates arc-shaped (concave upward) UBC curves; however, the application of L_3 loading results in the continuous rise of the p_u values as the annular section of the ring footing narrows down. These findings give the impression that ring footings are more beneficial for L_3 loading followed by L_2 and that followed by L_1 loading.

c) If the ground surface is surcharge less and the thickness of the sand layer ($\phi = 35°/40°$), is quite high ($h/r_0 \geq 5$), the UBC curves decrease at a considerable rate irrespective of the footing roughness and loading type; however, with the presence of surcharge pressure, the UBC curves, corresponding to high h/r_0 values, appear to be inverted 'V' shape when the loading is of L_3 type. For a particular sand-clay combination, the influence of surcharge pressure seems to be quite dominating in dictating the form of the UBC curves with respect to the radius ratio.

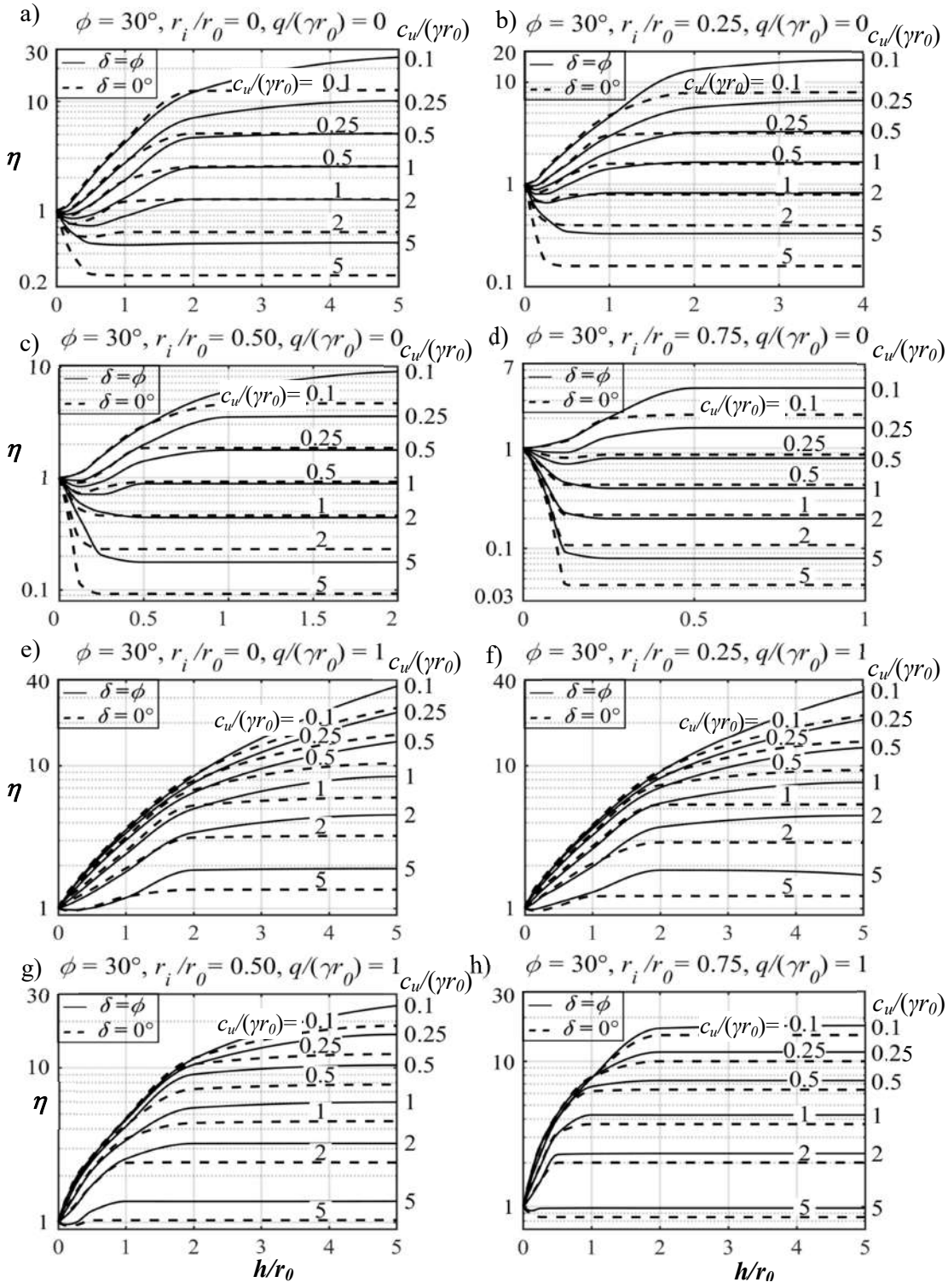

Figure 5.29 The variation of η with respect to h/r_0 for ring footing resting on sandy-clayey with (ϕ=30°) and corresponding to four different radius ratios: (a and e) r_i/r_0=0; (b and f) r_i/r_0=0.25; (c and g) r_i/r_0=0.50; and (d and h) r_i/r_0=0.75.

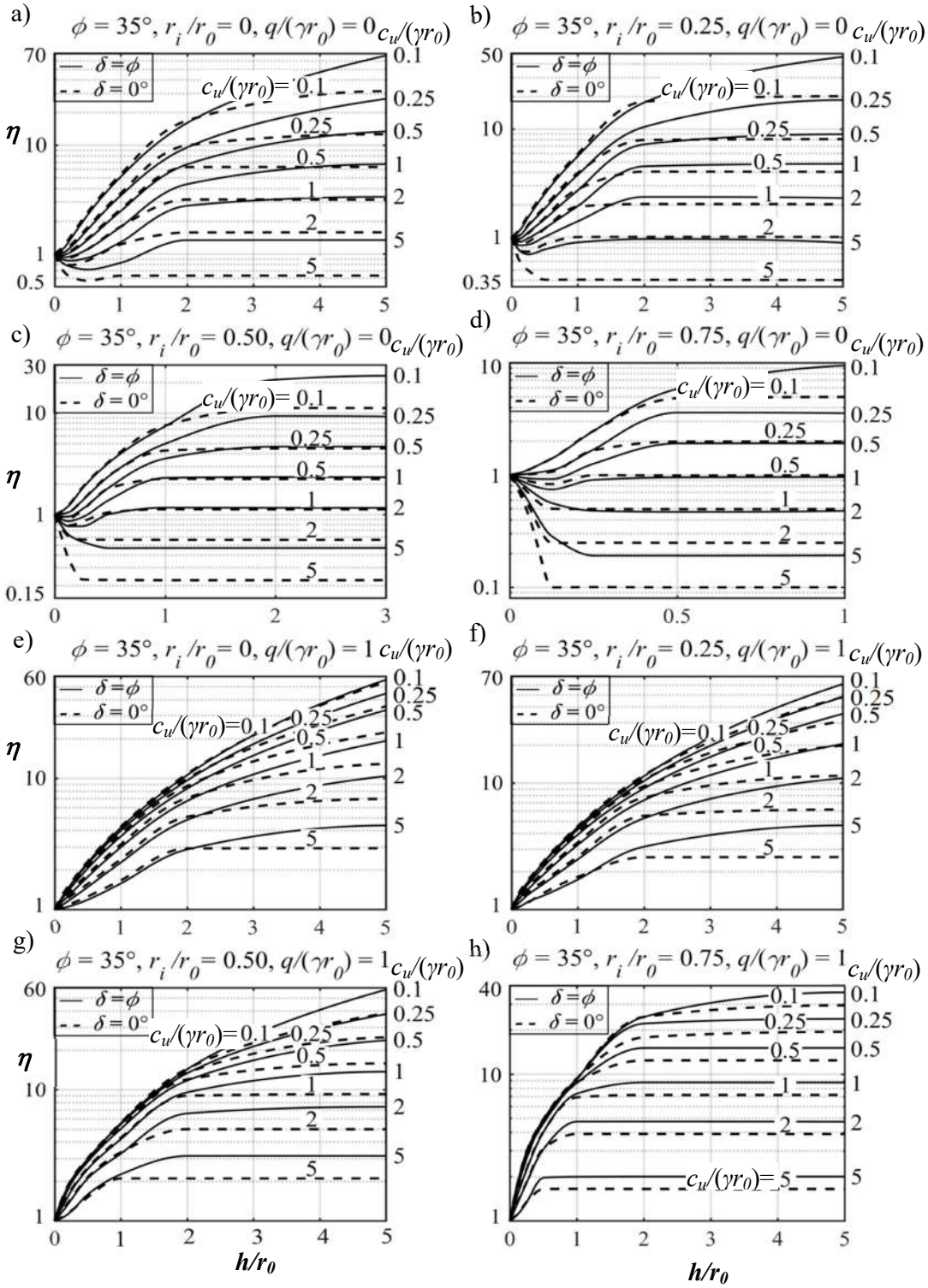

Figure 5.30 The variation of η with respect to h/r_0 for ring footing resting on sandy-clayey with (ϕ=35°) and corresponding to four different radius ratios: (a and e) r_i/r_0=0; (b and f) r_i/r_0=0.25; (c and g) r_i/r_0=0.50; and (d and h) r_i/r_0=0.75.

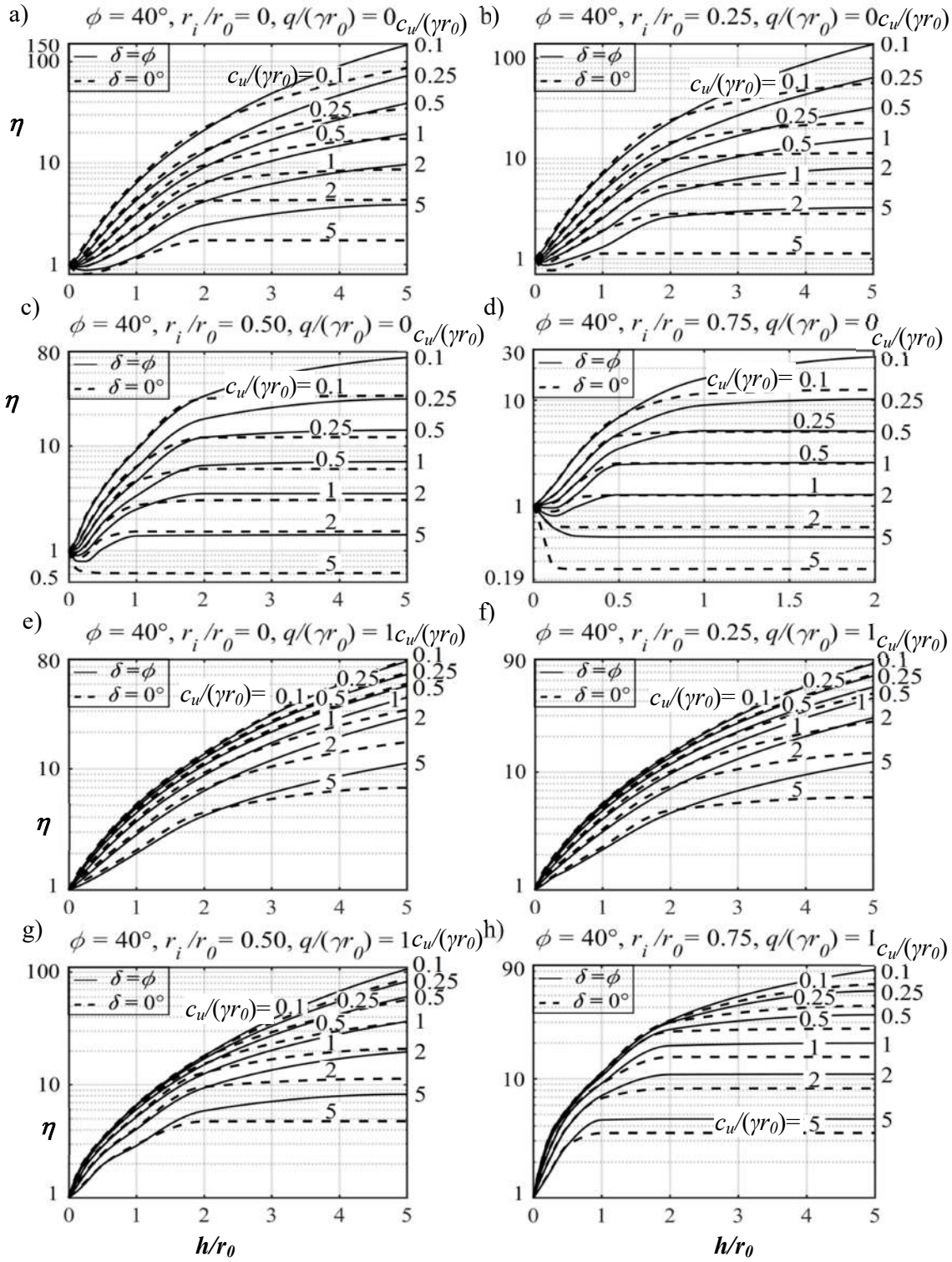

Figure 5.31 The variation of η with respect to h/r_0 for ring footing resting on sandy-clayey with (ϕ=40°) and corresponding to four different radius ratios: (a and e) r_i/r_0=0; (b and f) r_i/r_0=0.25; (c and g) r_i/r_0=0.50; and (d and h) r_i/r_0=0.75.

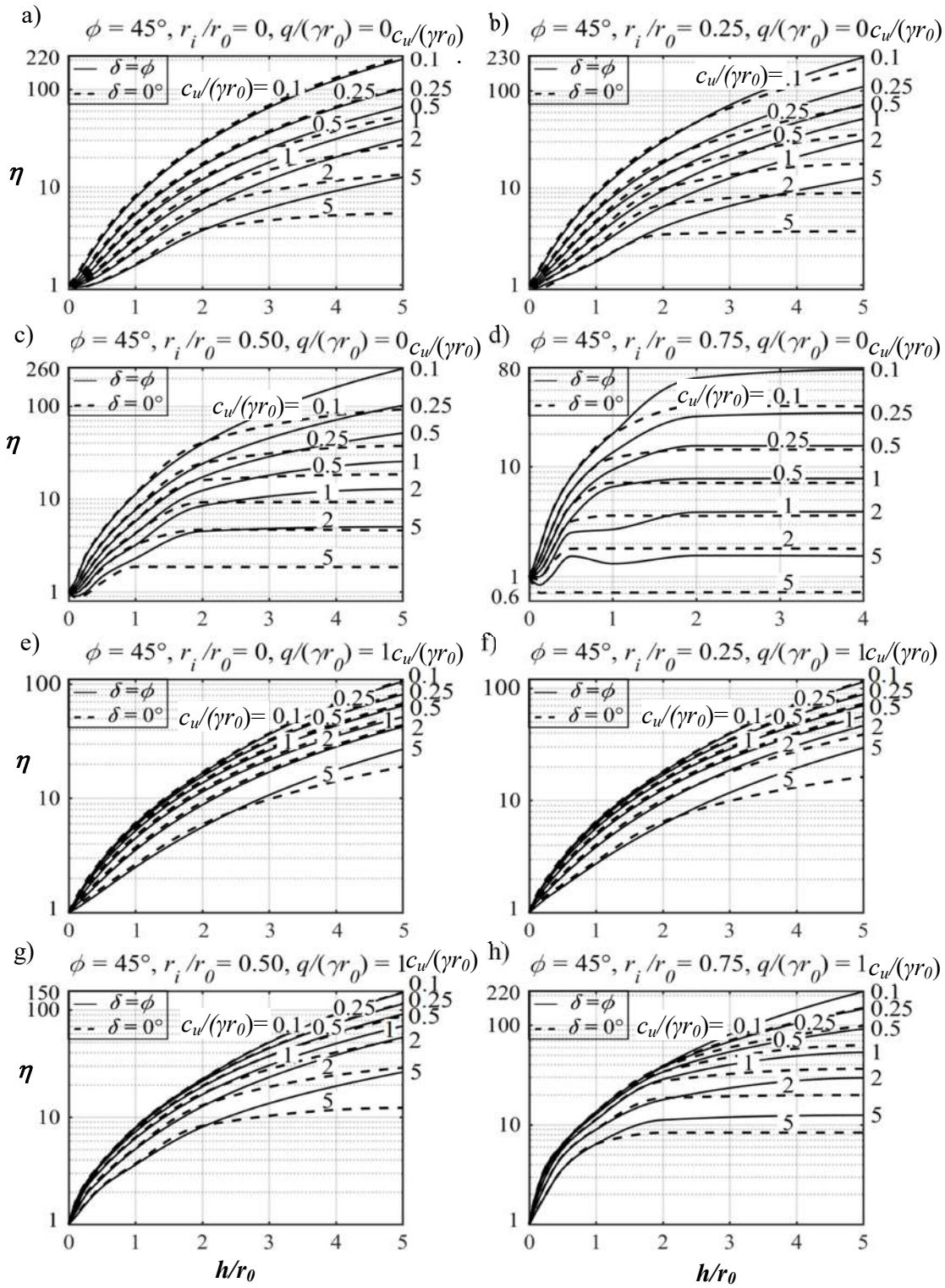

Figure 5.32 The variation of η with respect to h/r_0 for ring footing resting on sandy-clayey with (ϕ=45°) and corresponding to four different radius ratios: (a and e) r_i/r_0=0; (b and f) r_i/r_0=0.25; (c and g) r_i/r_0=0.50; and (d and h) r_i/r_0=0.75.

d) There are several UBC curves that initially increase (or remain to be the same) upto a certain r_i/r_0 and then subsequently decrease; this r_i/r_0, at which maximum p_u is noted is termed here as critical radius ratio ($r_i/r_0|_{cr}$). The $r_i/r_0|_{cr}$ becomes more prominent for L_3-type loading. Moreover, when a thick sand layer is sandwiched between the ring footing and undrained clays, the occurrence of $r_i/r_0|_{cr}$ is observed when an appreciable surcharge load acts over the ground surface. As the cohesive strength of the bottom clay layer increases and/or the drained friction angle of the top sand layer decreases, the magnitude of $r_i/r_0|_{cr}$ becomes smaller.

e) It can be inferred from these figures, that if the cohesive strength of the clay layer, lying below a relatively thinner sandy layer ($h/r_0 \leq 0.5$), is less than some specific $c_u/(\gamma r_0)$, denoted here as $c_u/(\gamma r_0)|_{sp}$, ring footings are preferable to the circular one. The magnitude of $c_u/(\gamma r_0)|_{sp}$ depends highly on the load type, surcharge pressure, and footing roughness. For the same material parameters and surcharge condition, $c_u/(\gamma r_0)|_{sp}$ appears to be maximum for L_3 type loading and notably smaller for L_1 type loading; for instance, if a surcharge-less sandy soil layer, having $\phi = 35°$, is placed beneath the rough footing with $h/r_0 = 0.5$, $c_u/(\gamma r_0)|_{sp}$ is reported to be 5, 1, and 0.125 for L_3, L_2, and L_1 loading type, respectively. The smooth footing further suppresses the value of $c_u/(\gamma r_0)|_{sp}$; nevertheless, the presence of surcharge pressure enhances the magnitude of $c_u/(\gamma r_0)|_{sp}$. Irrespective of the loading type, the usage of ring footing seems to be more beneficial in the presence of surcharge pressure, except for a small number of cases where a thin layer of sand is placed over a stronger cohesive soil ($c_u/(\gamma r_0) \geq 5$).

f) Depending on the layer strength and annular section, the bearing capacity of rough footing is evidently higher (or the same) than its smooth counterpart. The effect of footing roughness seems to be predominant for (a) surcharge-less soils, (b) larger radius ratio, (c) higher sand layer thickness, (d) lower strength of sand layer, and (e) relatively high strength of the bottom undrained cohesive layer. The UBC profiles corresponding to smooth and rough footings coincide with each other when the undrained cohesive strength of the bottom clay layer is quite less. This difference of p_u between the smooth and rough footing escalates when a small-width ring footing is placed on relatively weaker sands overlying stronger clays regardless of the loading condition. However, the variation of p_u due to the footing roughness seems to be unaffected by the loading position.

g) Regardless of the footing roughness condition, the influence of the strength of the lower layer on UBC diminishes with the increase in top layer thickness. This is reflected by the merging of the UBC curves related to various values of undrained cohesion of the bottom layer when the surcharge does not act on the thick overlying sandy layer. In the presence of surcharge pressure, this merger occurs at a relatively higher r_i/r_0 ratio, and the deviation of the UBC curves for the lower r_i/r_0 ratio is predominant for L_3 loading than its L_1 counterpart. Apparently, there exists a certain sand (top) layer thickness beyond which the bearing capacity of the footing is dictated by the sand layer alone; this specific thickness is defined here as optimum thickness, and in the normalized form it is designated as h_{opt}/r_0. The h_{opt}/r_0 becomes easier to obtain from the efficiency factor profiles, as shown in Figures 5.29 to 5.32.

h) In most cases, with the increase in sand layer thickness, there is a significant improvement in UBC, especially when the added sand layer is of higher

strength. Initially, the η-profiles increase at a considerable rate and eventually attain a horizontal plateau; this manifests the existence of h_{opt}/r_0. Table 5.5 presents the variation of h_{opt}/r_0 corresponding to different soil combinations, various sized-ring footing, and in the presence/absence of surcharge pressures. The magnitude of h_{opt}/r_0 is higher for the rough footing and it further increases with the (a) increase in ϕ of the top layer, (b) decrease in cohesive strength of the bottom layer, and (c) in the presence of surcharge pressure. The deviation between the η-profiles generated from the smooth and the rough footing becomes wider as the sand layer thickness increases. The action of surcharge pressure reduces the spread of η-profiles pertaining to the least and the maximum cohesive soils. Further, the loading position does not have any influence on the computed η-value.

Table 5.5. The variation of h_{opt}/r_0 corresponding to different values of ϕ, $c_u/(\gamma r_0)$, r_i/r_0, and $q/(\gamma r_0)$.

ϕ	r_i/r_0	h_{opt}/r_0					
		$c_u/(\gamma r_0)$ =0.25		$c_u/(\gamma r_0)$ =1		$c_u/(\gamma r_0)$ =2	
		$q/(\gamma r_0)$=0	$q/(\gamma r_0)$=1	$q/(\gamma r_0)$=0	$q/(\gamma r_0)$=1	$q/(\gamma r_0)$=0	$q/(\gamma r_0)$=1
35º	0	9.0 (5.0)	10 (8.5)	6.0 (2.0)	10 (7.0)	5.0 (1.8)	7.0 (6.0)
	0.25	5.5 (2.5)	9.5 (8.0)	4.5 (2.0)	8.5 (5.0)	2.0 (1.5)	6.0 (5.0)
	0.50	2.0 (1.1)	8.0 (7.0)	2.0 (1.0)	6.0 (2.0)	1.2 (0.3)	5.0 (2.0)
	0.75	1.0 (0.5)	4.5 (4.0)	0.75 (0.25)	2.0 (1.0)	0.25 (0.12)	1.5 (1.0)
45º	0	>10 (9.0)	>10 (>10)	>10 (8.8)	>10 (>10)	>10 (8.0)	>10 (10)
	0.25	>10 (8.0)	>10 (>10)	10 (6.0)	>10 (>10)	10 (7.0)	>10 (8.0)
	0.50	9.0 (5.5)	>10 (>10)	6.5 (2.0)	>10 (9.5)	5.0 (2.0)	10 (6.0)
	0.75	5.0 (2.0)	>10 (10)	2.0 (1.0)	10 (8.8)	2.0 (0.5)	6.5 (2.5)

Note: The values inside and outside the parenthesis correspond to smooth and rough footing, respectively.

i) However, there are a few cases where η profiles are declining. This occurs when a thin ring footing is placed over relatively weaker sands, without surcharging, and underlain by stronger clays. For an instance, the η-profile suggests that sand, with ϕ=35°, is not recommended to place over cohesive soil with $c_u/(\gamma r_0)\geq 0.5$, if the ring footing, having r_i/r_0 =0.75, is placed over surcharge less ground surface.

5.3.3 Failure patterns

The statically admissible stress field, obtained at the incipient of the collapse state, is used for developing the failure contours. For each node, the radius of the Mohr circles corresponding to the failure state (*d*) and the current state of stress (*a*) are obtained as mentioned in Section 4.5. As the Tresca criterion is utilized to model the undrained, saturated clays, it follows that the parameter *d* equals the cohesion of the soil at that point. The proximity of the stress state with respect to shear failure is characterized by *a/d* ratio, as mentioned in Section 4.5.

Influence of loading positions

Corresponding to the three loading positions, the plastic failure contours are drawn for three different layered soils: (i) Type A2 of S–S case (having ϕ_1 = 45° and ϕ_2 = 30°) (ii) Type B2 of C–C case ($c_{u1}/(\gamma r_0)$ = 1 and $c_{u2}/(\gamma r_0)$ = 0.5), and (iii) S–C case (having ϕ = 40° and $c_u/(\gamma r_0)$ = 0.5). The contours are presented in Figure 5.33. A non-plastic rigid wedge seems to develop beneath the footing base. Although there is a noticeable change in the shape of the failure surfaces, however, the horizontal extent and the overall size of the failure zone appear to be unaffected by the loading positions.

Influence of radius ratios

The influence of the radius ratio on the failure zone is displayed in Figure 5.34 for soil Type A2 and Type B2. This reduction is far more significant in sand-sand

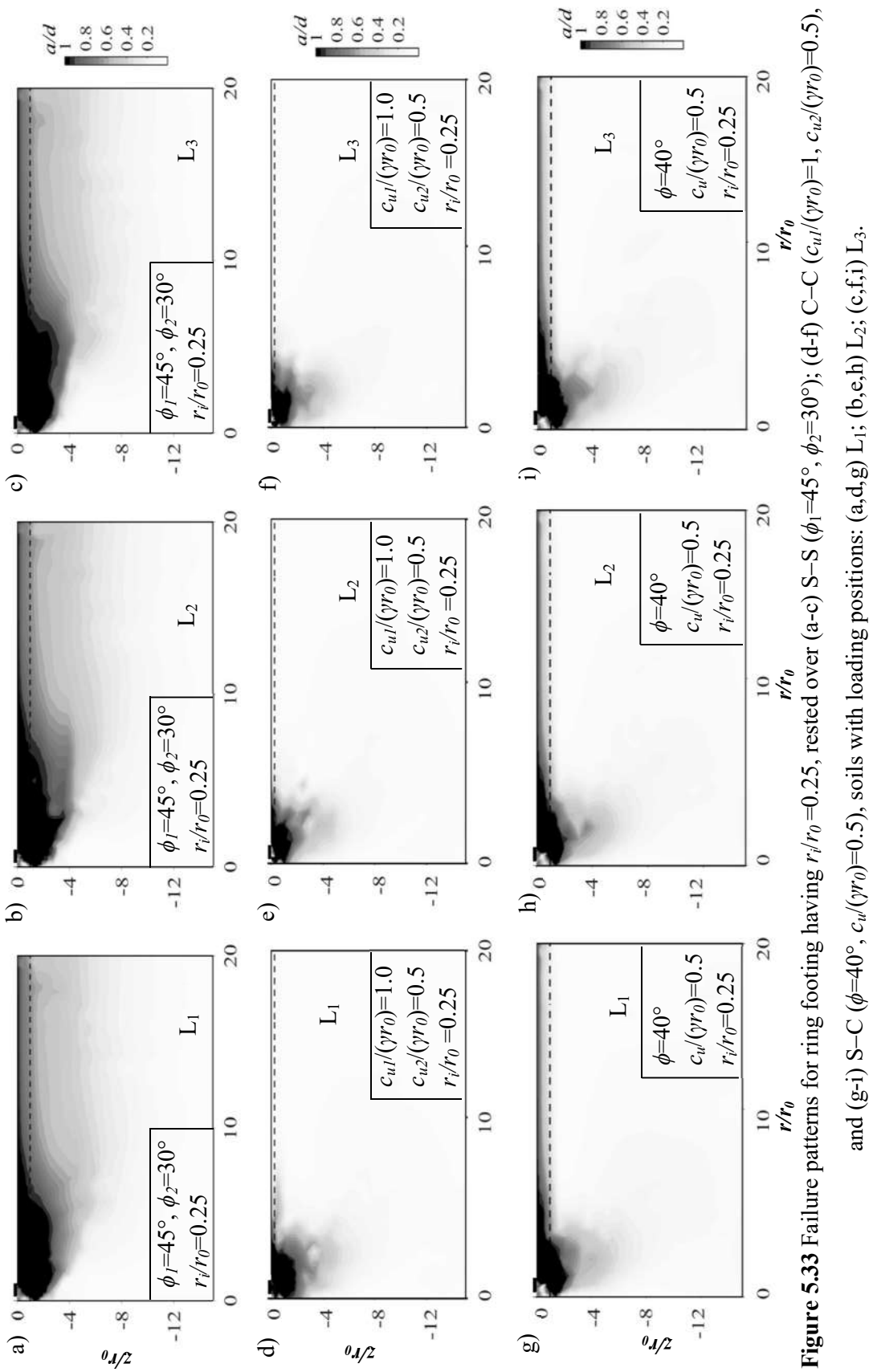

Figure 5.33 Failure patterns for ring footing having r_i/r_0 =0.25, rested over (a-c) S–S (ϕ_1=45°, ϕ_2=30°); (d-f) C–C ($c_{u1}/(\gamma r_0)$=1, $c_{u2}/(\gamma r_0)$=0.5), and (g-i) S–C (ϕ=40°, $c_u/(\gamma r_0)$=0.5), soils with loading positions: (a,d,g) L_1; (b,e,h) L_2; (c,f,i) L_3.

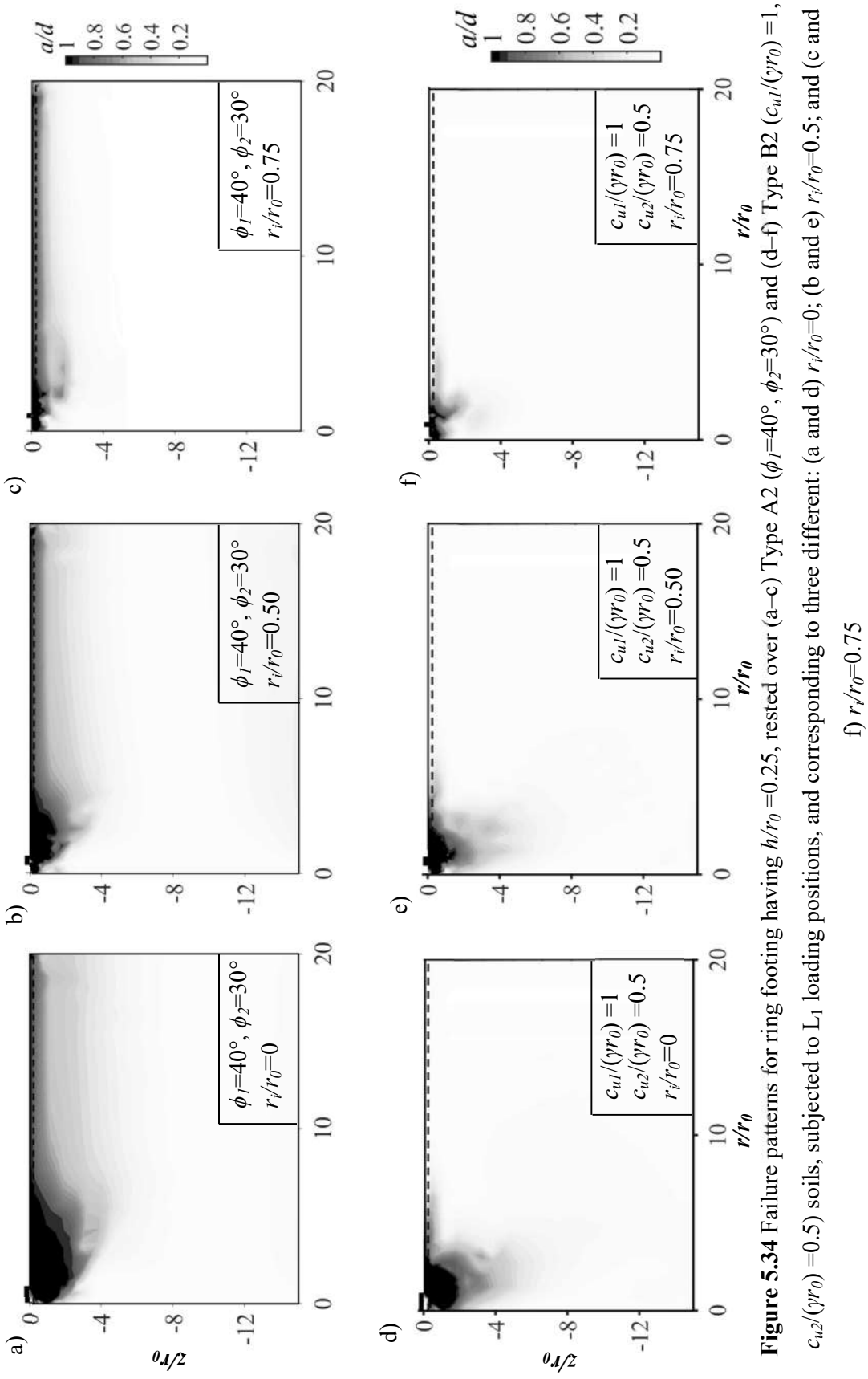

Figure 5.34 Failure patterns for ring footing having h/r_0 =0.25, rested over (a–c) Type A2 (ϕ_1=40°, ϕ_2=30°) and (d–f) Type B2 ($c_{u1}/(\gamma r_0)$ =1, $c_{u2}/(\gamma r_0)$ =0.5) soils, subjected to L_1 loading positions, and corresponding to three different: (a and d) r_i/r_0=0; (b and e) r_i/r_0=0.5; and (c and f) r_i/r_0=0.75

system in comparison to its clay-clay counterpart. This observation further corroborates the numerical findings that the UBC of the ring footing reduces as the width of the annular section decreases.

The effect of the ring sizes on the form and the extent of the failure zone, corresponding to sand-clay layered system, is displayed in Figure 5.35. The failure contours are drawn for four radius ratios, namely, r_i/r_0 = 0, 0.25, 0.50, and 0.75; the rest of the chosen parameters are kept constant ($c_u/(\gamma r_0)$ = 1, q = 0, h/r_0 = 1, and ϕ = 35°). Corresponding to the chosen strength combinations and the upper layer thickness, the figure shows that the encompassed soil volume within the failure surface becomes maximum for r_i/r_0 = 0.25 and thereafter, the failure zone shrinks and the size of the plastic zone reduces to a very small portion adjacent to the footing surface when r_i/r_0 = 0.75. The shrinking in the failure zone reinforces the existence of $r_i/r_0|_{cr.}$ As the width of the ring reduces, there is the generation of two shear bulbs. With the thinning in the ring footing, the shear bulbs approach symmetricity which, resembles the failure pattern developed below the strip footing. Therefore, for a very high value of r_i/r_0, ring footing starts to behave as a strip footing.

Influence of upper layer thickness

Figure 5.36 presents the failure zones develops within a certain soil Type A2 of S–S case (ϕ_1 = 40° and ϕ_2 = 35°) corresponding to four different values of h/r_0, namely, 0.5, 1, 2, and 5. The width of the ring footing and the loading condition are kept the same. It can be clearly seen that after a certain h/r_0, plastic failure zone remains confined only within the top layer. This explains the reason of the existence of h_{opt}/r_0.

Figure 5.37 shows the failure patterns by varying the thickness of the top sand layer for S–C case. By enforcing the constancy of the other input parameters, three thicknesses are chosen (namely, h/r_0 = 0.5, 2, and 4) for the simulations. As the sand

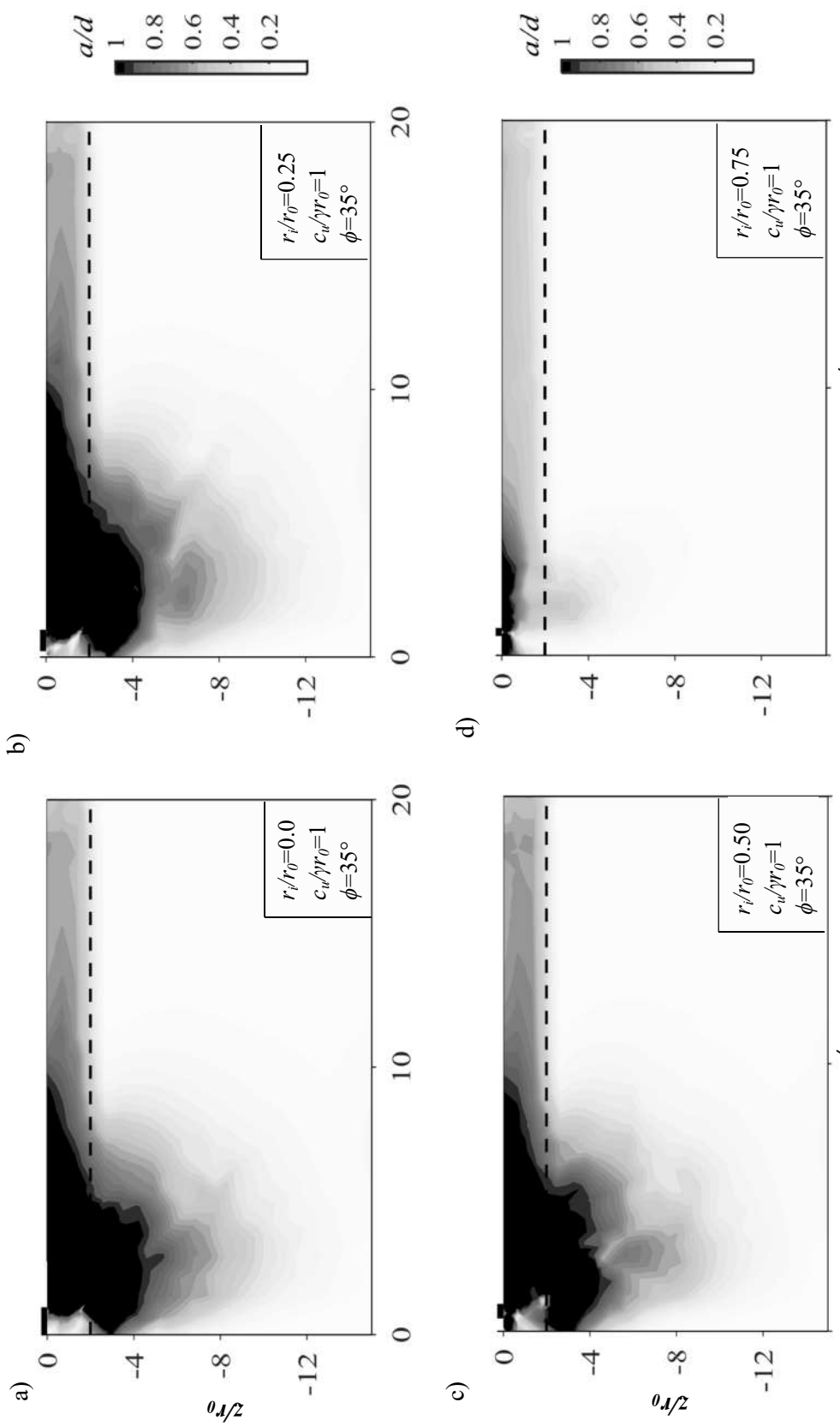

Figure 5.35 Failure pattern for ϕ=35°, $c_u/(\gamma r_0)$=1, h/r_0=2, and $q/(\gamma r_0)$=1 with: a) r_i/r_0= 0; b) r_i/r_0=0.25; c) r_i/r_0=0.5; and d) r_i/r_0=0.75.

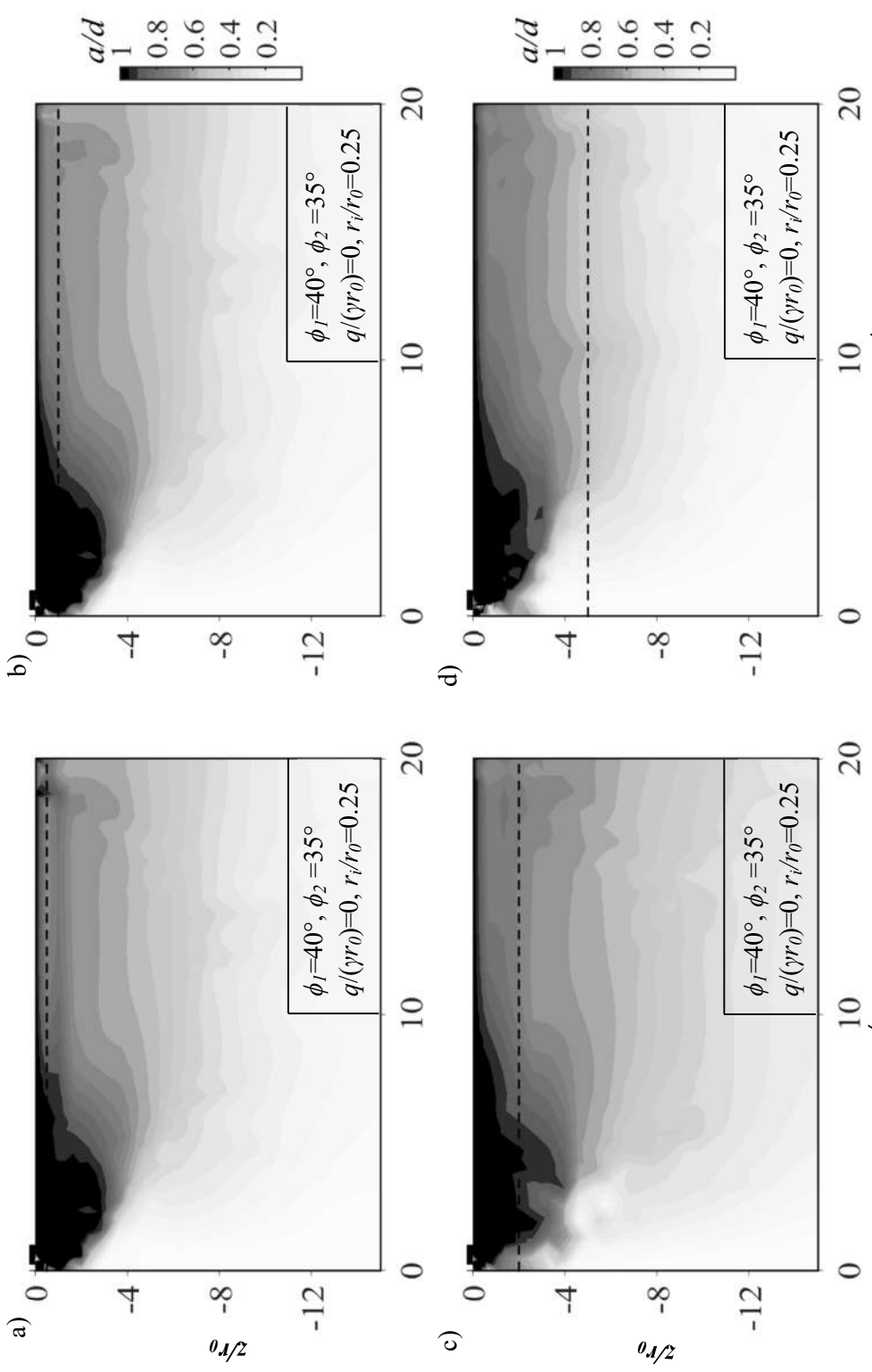

Figure 5.36 Failure patterns for ring foundation having ϕ_1=40°, ϕ_2 =35°, r_i/r_0=0.25, and $q/(\gamma r_0)$=0 subjected to L_2 loading position, and corresponding to: a) h/r_0=0.5; b) h/r_0=1; c) h/r_0=2; and d) h/r_0=5.

layer thickness increases, the size of the plastic shear zone decreases and gets limited within the top layer. There is also a development of the double shear bulbs with the increase in sand layer thickness.

Influence of strength parameters for sand-clay layered system

Figure 5.38 illustrates the form of the failure patterns for three different overlying sand layers, namely, $\phi = 35°$, $\phi = 40°$, and $\phi = 45°$; the rest of the parameters ($c_u/(\gamma r_0) = 1$, q=0, $h/r_0 = 2$, and $r_i/r_0 = 0.25$) are kept to be constant. The figures give an impression that with the increase in the strength of the sand, the overall volume of the plastic zone encompassed within the failure surface increases to a significant extent.

Figure 5.39 demonstrates how the size and shape of the failure zone get impacted by the cohesive strength of the bottom layer. The size of the failure zone decreases extensively as there is an improvement in the undrained strength of the bottom layer. For $c_u/(\gamma r_0) = 0.1$, the plastic zone enters the lower layer, whereas, when the strength of the bottom clays is quite high ($c_u/(\gamma r_0) =10$), the plastic zone is well contained within the upper layer. The continuity of the curvilinear failure surface gets highly affected when a stronger sand layer is placed over a weaker clayey stratum. In most of the cases, the extension of the failure zone remains much greater in the lateral direction as compared to its vertical counterpart. Nevertheless, when the bottom clayey layer is extremely weak, the extension of the failure zone becomes more in the vertical downward direction. It can be summarized that the size of the failure zone enlarges due to the (a) increase in the drained strength of the top sand layer and/or (b) decrease in the undrained strength of the underlying clay layer. In a nutshell, the form and the overall extent of the failure pattern gets highly impacted by the strength and the thickness of the underlying layers and the ring footing width but the loading position hardly influences the failure pattern.

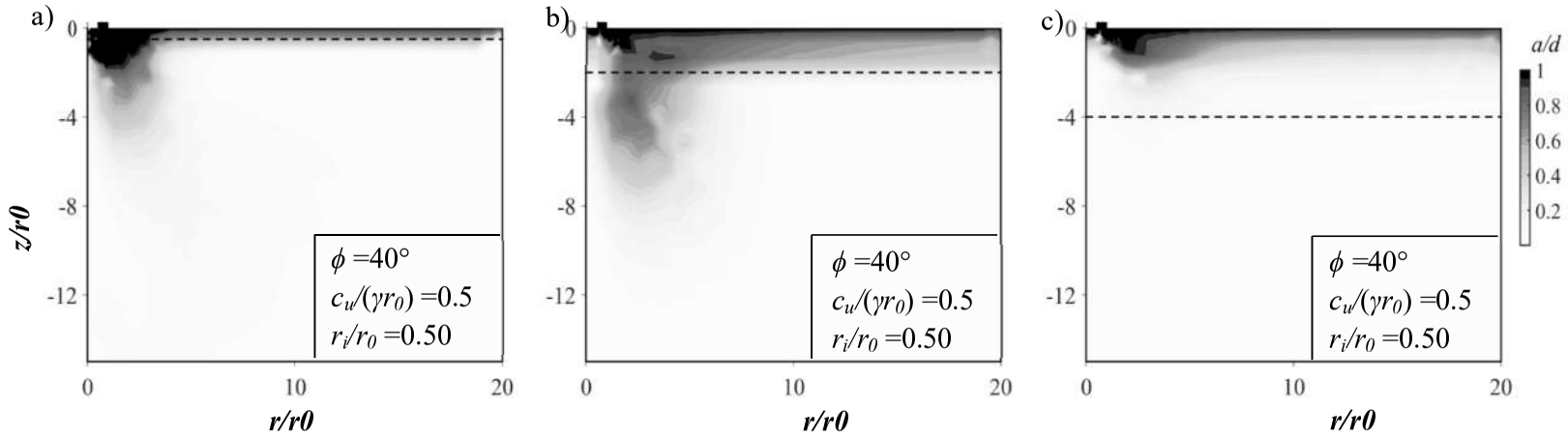

Figure 5.37 Failure patterns for ring foundation having ϕ=40°, $c_u/(\gamma r_0)$ =0.5, r_i/r_0 =0.50, and $q/(\gamma r_0)$=0, subjected to L_2 loading position, and corresponding to: a) h/r_0=0.5; b) h/r_0=2; and d) h/r_0=4.

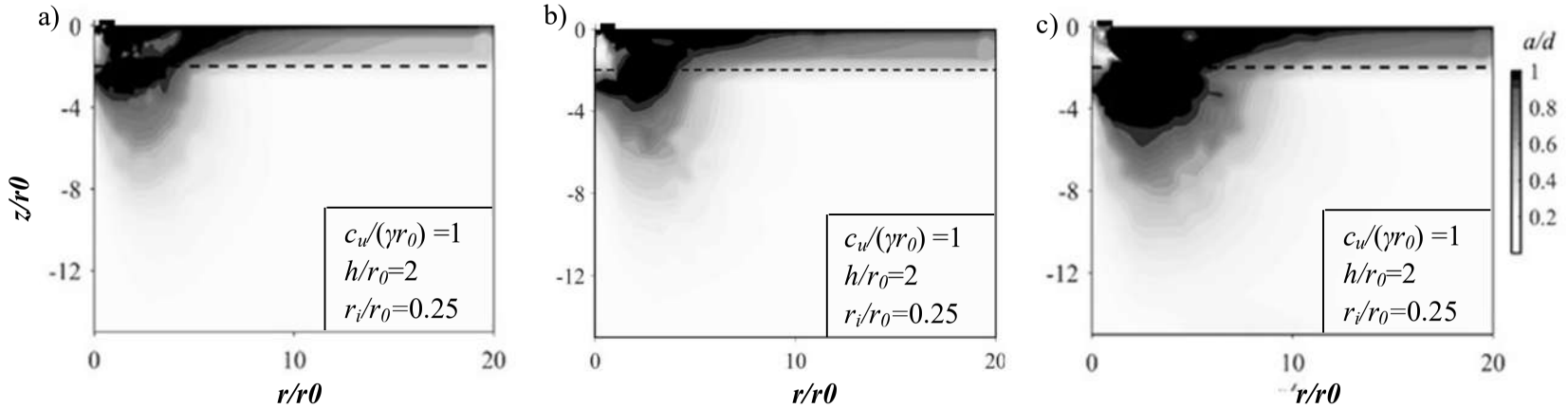

Figure 5.38 Failure patterns for ring foundation having $c_u/(\gamma r_0)$ =1, h/r_0=2, and r_i/r_0 =0.25, subjected to L_2 loading position, and corresponding to: a) ϕ =35°; b) ϕ =40°; and c) ϕ=45°.

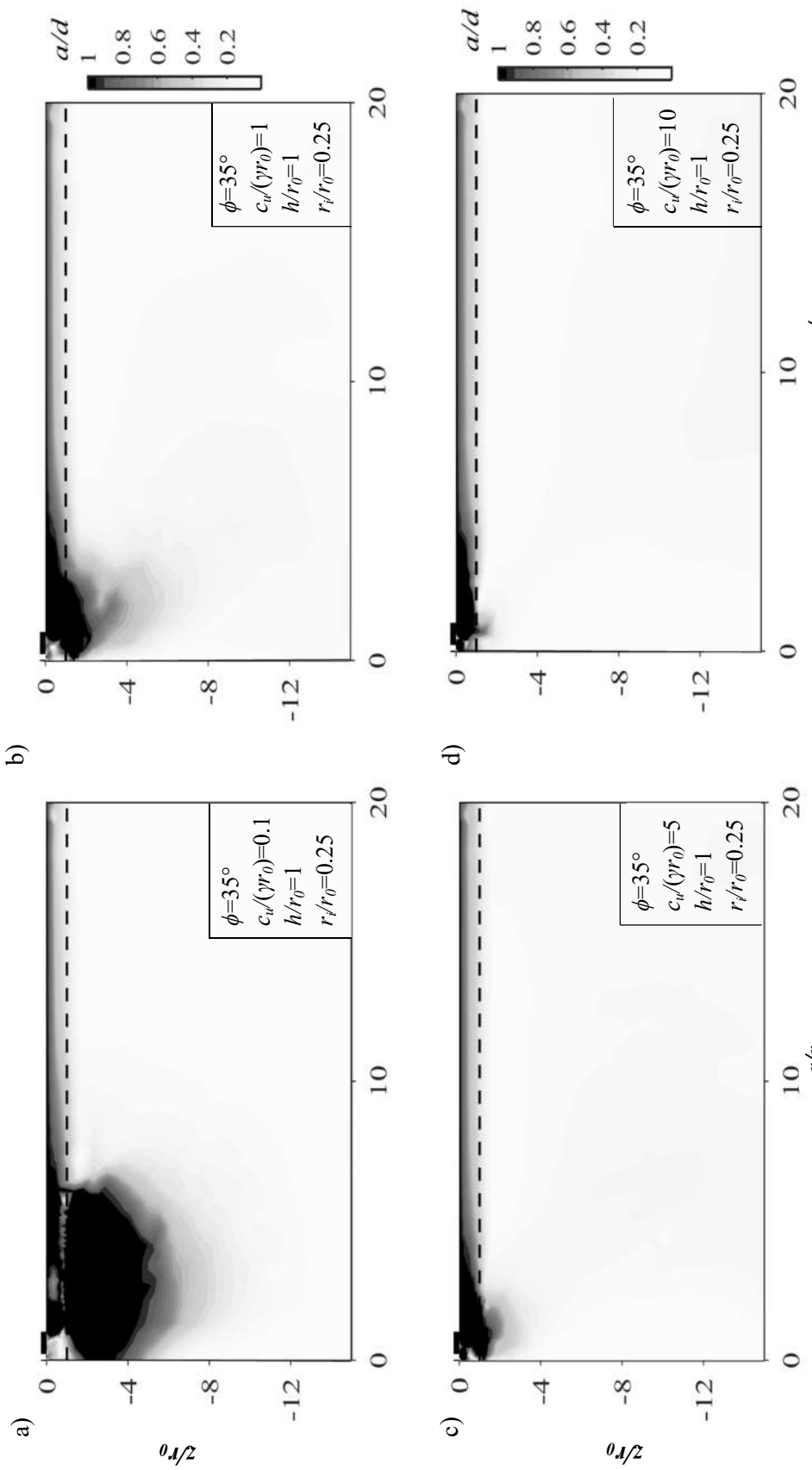

Figure 5.39 Failure patterns for ring foundation having ϕ=35°, h/r_0=1, and r_i/r_0 =0.25, subjected to L_2 loading position, and corresponding to: a) $c_u/(\gamma r_0)$=0.1; b) $c_u/(\gamma r_0)$=1; c) $c_u/(\gamma r_0)$=5; and d) $c_u/(\gamma r_0)$=10.

5.4 COMPARISONS OF RESULTS

A detailed comparative study of the circular and ring footing was shown earlier in Section 4.6 corresponding to L_0 loading. Evidently, circular footing ($r_i/r_0 = 0$) is a special type of ring footing. The computed UBC of ring footings, rested on homogeneous (cohesionless frictional soil and undrained saturated cohesive soil) as well as layered soil, were compared with the available solutions obtained by using various analytical and numerical methods. The present non-linear lower bound technique improves the solutions reported earlier by linearizing the yield criterion. Moreover, the present results are found to be in well accordance with the results obtained by using OptumG2. The closeness of the computed and the reported solutions provides confidence in the adopted methodology and the written code.

In this section, the comparative study is extended for two more cases: (a) ring footing subjected to L_0 loading and rested over layered system (S–S and C–C), and (b) ring footing subjected to partial loading and rested over homogenous frictional and cohesive soils.

5.4.1 For L_0 loading and layered system

The N_c values of the ring footing computed from the present analysis are compared with the solutions provided by Lee et al. (2016) based on finite-element software, Plaxis and listed in Table 5.6. For soil Type B1, the present values appear to be higher than the solutions of Lee et al. (2016). However, when stronger undrained clays are laid over weaker clays, the solutions from the present analysis are smaller than the finite-element solutions. Table 5.7 further presents the comparison of N_γ values with the solutions provided by Khatri et al. (2020) and Das et al. (2021) for Type A1 as well as Type A2 soil. The present values match quite well with the available solutions.

Table 5.6. A comparison of N_c values for ring footing on clay–clay layer for L_0 loading

h/r_0	c_{u1}/c_{u2}	Present study[a]				Lee et al. (2016)[b]			
		r_i/r_0				r_i/r_0			
		0	0.25	0.5	0.75	0	0.25	0.5	0.75
0.125	0.5	8.38	7.74	6.69	5.75	7.32	6.38	5.71	5.40
	2.0	3.44	4.07	4.02	4.41	3.84	4.06	4.20	4.98
	4.0	1.96	2.78	2.85	3.26	2.36	2.53	2.98	3.86
0.25	0.5	6.53	6.54	5.95	5.67	6.28	5.93	5.62	5.40
	2.0	4.59	4.52	4.63	5.32	4.52	4.80	5.38	5.40
	4.0	2.64	3.16	3.85	5.13	3.08	3.30	4.09	5.40
0.50	0.5	6.22	6.18	5.89	5.68	6.08	5.93	5.61	5.40
	2.0	4.47	5.19	5.69	5.68	5.60	5.93	5.61	5.40
	4.0	3.70	3.86	4.59	5.67	4.32	4.61	5.61	5.40

Note: a: The solutions are obtained based on LB FELA with the help of IPM by smoothening the yield criterion.
b: The solutions are obtained based on finite-element method by using the Plaxis software.

Table 5.7. A comparison of N_γ values for ring footing on sand–sand layered soil for L_0 loading

r_i/r_0	h/r_0	$\phi_1 = 40°, \phi_2 = 30°$			$\phi_1 = 40°, \phi_2 = 30°$	
		Present study[a]	Khatri et al. (2020)[b]	Khatri et al. (2020)[c]	Present study[a]	Das et al. (2021)[b]*
0	0.25	21.37	20.74	21.58	46.87	47.68
	0.50	30.27	29.56	30.66	24.46	22.73
	1.00	52.01	50.10	52.38	13.00	12.27
	2.00	104.91	103.40	109.62	--	--
0.25	0.25	29.38	27.27	29.46	20.15	19.50
	0.50	42.96	41.55	43.61	11.41	10.80
	1.00	73.62	71.51	74.42	10.95	9.62
	2.00	123.31	124.14	140.82	--	--
0.50	0.25	24.93	24.60	26.40	9.60	8.77
	0.50	48.54	47.84	51.64	8.32	7.59
	1.00	77.97	77.48	87.20	8.30	7.51

Note: a: The solutions are obtained based on LB FELA with the help of IPM by smoothening the yield criterion.
b: The solutions are obtained based on LB limit theorems by using the Optum G2 software.
c: The solutions are obtained based on UB limit theorems by using the Optum G2 software.
*The values are extracted from curves.

5.4.2 For partial loading and homogenous soils

Corresponding to different loading conditions and two different soil-footing interfaces, Table 5.8 presented comprehensive comparisons of N_c and N_γ values for ring footing placed over homogenous soils with the numerical solutions provided by Vali et al. (2019) through Optum G2 software. The N_c values are compared for undrained clays having $c_u/(\gamma r_0)$ =1, and N_γ values were evaluated for two drained sands having ϕ equals to 30° and 40°. The present results were in good agreement with the solutions provided by Vali et al. (2019). The little discrepancies between both the solutions may be because of the difference between the meshing and the chosen tolerance limit.

5.5 LIMITATIONS

Along with the vertical loads, ring footings are also susceptible to the horizontal loads (e.g., wind loads) due to the ring footings being mainly used for transmitting the load of the tall structures to the ground. Hence, in order to simulate real-life field problems, inclined loadings are required to be considered in the analysis of ring footing (Sharma and Kumar, 2017); nevertheless, similar to most of the existing literatures, the present article does not include the lateral loads in the numerical analysis. Moreover, the present study is carried out solely by using the lower-bound limit theorem in which statically admissible stress fields are constructed and subsequently analysed to obtain the safe collapse load based on perfectly plastic material, coaxiality, and associated flow rule. There is no consideration of the strain or displacement field in this analysis. Unlike displacement-based elastoplastic FEM, limit theorems neither use any stiffness parameter nor require adoption of any constitutive model, and, hence, load-settlement curves are not possible to obtain in the present study.

Table 5.8. A comparison of N_c and N_γ for ring footing resting on homogenous soils for different loading positions.

Loading Position	r_i/r_0	N_c				N_γ							
		Present study[a]		Vali et al.(2019)[b]		Present study[a]				Vali et al.(2019)[b]			
		$c_u/(\gamma r_0)$=1				ϕ =30°		ϕ =40°		ϕ =30°		ϕ =40°	
		rough	smooth	rough	smooth	rough	smooth	rough	smooth	rough	smooth	rough	smooth
L_1	0.00	24.09	22.72	24.09	22.63	60.64	28.65	463.61	196.08	58.84	27.78	462.06	191.57
	0.25	16.80	15.90	--	--	42.02	19.22	407.70	135.50	--	--	--	--
	0.50	13.33	12.97	13.34	12.96	31.41	15.91	250.59	103.93	30.43	15.05	251.70	101.46
	0.75	11.43	11.32	11.47	11.30	28.83	15.58	182.78	90.61	27.50	14.18	181.84	87.18
L_2	0.00	12.05	11.36	12.05	11.33	30.40	14.30	231.77	97.66	30.03	14.03	236.82	96.36
	0.25	11.73	11.11	--	--	29.82	13.49	289.34	95.50	--	--	--	--
	0.50	11.11	10.80	11.13	10.81	26.62	13.31	210.26	87.76	25.98	12.68	214.72	86.85
	0.75	10.61	10.24	10.65	10.52	27.16	33.67	169.36	84.88	26.05	13.04	174.34	82.09
L_3	0.00	8.03	7.56	8.03	7.54	20.04	9.48	152.46	64.92	19.61	9.26	152.97	63.93
	0.25	9.03	8.55	--	--	22.62	10.30	218.78	73.09	--	--	--	--
	0.50	9.50	9.26	9.53	9.11	22.53	11.34	177.565	73.77	21.62	10.77	178.70	72.44
	0.75	9.91	9.80	9.94	9.79	24.92	13.45	159.398	78.33	23.83	12.33	159.59	75.22

Note: a: The solutions are obtained on the basis of finite element lower bound theorem by smoothening the yield criterion and using IPM.
b: The solutions are obtained on the basis of FELA software, Optum G2.

5.6 SUMMARY

The present study focuses on investigating the ultimate bearing capacity of the partially-loaded ring footing resting over various layered soils. The numerical simulations are carried out by using the axisymmetric lower bound limit analysis in combination with finite elements and IPM-based non-linear optimization. Three different partial loadings, namely, inner half loading, middle half loading, and outer half loading are considered in the analysis. An extensive investigation is carried out to understand the combined effect of loading positions, strength properties of different layers, upper layer thickness, surcharge pressure, ring size, and footing roughness. The results are presented in terms of normalized bearing capacity and efficiency factor. The normalized bearing capacity of ring footing subjected to complete loading is always found to be minimum from the UBC obtained from partial loadings. Within the partial loading; inner half loading manifests the maximum benefits in terms of load withstanding. The efficiency factor is expressed as the ratio of the bearing capacity of a ring footing in the presence of an upper layer to the bearing capacity of a ring footing placed exclusively on a homogeneous bottom layer. This study evinced the development of following four threshold parameters for some cases. These threshold parameters are: optimum upper layer thickness, specific radius ratio, critical radius ratio, and specific cohesive strength. The optimum upper layer thickness is the thickness beyond which the bearing capacity of the footing becomes independent of the lower soil strength. The critical radius ratio is defined as the radius ratio at which the soil's bearing capacity is maximum. The specific radius ratio is the radius ratio beyond which the bearing capacity solely depends on the strength of the upper layer. The specific cohesive strength is defined as the cohesive strength beyond which ring footings are preferred over circular footings for relatively thinner sand layers. The efficiency factor

and optimum layer thickness of the upper layer are independent of loading positions. To further corroborate the numerical findings, failure patterns illustrating the trend and the extent of the plastic shear zone are drawn for a few cases. The design charts presented in this chapter may be useful to practicing engineers. The failure contours drawn at the incipient of collapse further reinforce the numerical findings.